OXFORD UNIVERSITY PRESS | Toxicological Sciences

Exploring the effects of topoisomerase II inhibitor XK469 on anthracycline cardiotoxicity and DNA damage

Journal:	*Toxicological Sciences*
Manuscript ID	TOXSCI-23-0342.R2
Manuscript Type:	Research Article
Date Submitted by the Author:	n/a
Complete List of Authors:	Kerestes, Veronika; Charles University Faculty of Pharmacy in Hradec Kralove Kubes, Jan; Charles University Faculty of Pharmacy in Hradec Kralove Applova, Lenka; Charles University Faculty of Pharmacy in Hradec Kralove Kollarova, Petra; Charles University Faculty of Medicine in Hradec Kralove Lencova-Popelova, Olga; Charles University Faculty of Medicine in Hradec Kralove Melnikova, Iuliia; Charles University Faculty of Pharmacy in Hradec Kralove Karabanovich, Galina; Charles University Faculty of Pharmacy in Hradec Kralove Khazeem, Mushtaq M.; University of Mustansiriyah National Center of Hematology Bavlovic-Piskackova, Hana; Charles University Faculty of Pharmacy in Hradec Kralove Kovarikova, Petra; Charles University Faculty of Pharmacy in Hradec Kralove Austin, Caroline A.; Newcastle University Biosciences Institute Roh, Jaroslav; Charles University Faculty of Pharmacy in Hradec Kralove Sterba, Martin; Charles University Faculty of Medicine in Hradec Kralove Simunek, Tomas; Charles University Faculty of Pharmacy in Hradec Kralove Jirkovska, Anna; Charles University Faculty of Pharmacy in Hradec Kralove
Category - Please select one category that is most applicable to your manuscript.:	Organ Specific Toxicology
Key Words:	anthracycline cardiotoxicity, topoisomerase II, XK469

Exploring the effects of topoisomerase II inhibitor XK469 on anthracycline cardiotoxicity and DNA damage

Veronika Kereseš[1], skalicv1@faf.cuni.cz, ORCID ID: 0000-0003-0929-7376

Jan Kubeš[1], kubesja1@faf.cuni.cz, ORCID ID: 0000-0002-0513-4847

Lenka Applová[1], applovl@faf.cuni.cz, ORCID ID: 0000-0001-6740-9685

Petra Kollárová[2], petra.kollarova@lfhk.cuni.cz, ORCID ID: 0000-0001-9673-9210

Olga Lenčová-Popelová[2], lencovao@lfhk.cuni.cz, ORCID ID: 0000-0001-7178-8470

Iuliia Melnikova[1], melnikoi@faf.cuni.cz, ORCID ID: 0000-0002-5378-4764

Galina Karabanovich[1], karabang@faf.cuni.cz, ORCID ID: 0000-0001-5923-7553

Mushtaq M. Khazeem[3], m.m.khazeem@uomustansiriyah.edu.iq, ORCID ID: 0000-0003-2948-8225

Hana Bavlovič Piskáčková[1], piskacha@faf.cuni.cz, ORCID ID: 0000-0002-9817-7247

Petra Štěrbová-Kovaříková[1], kovarikova@faf.cuni.cz, ORCID ID: 0000-0002-1242-5706

Caroline A. Austin[4], caroline.austin@newcastle.ac.uk, ORCID ID: 0000-0002-1921-5947

Jaroslav Roh[1], rohj@faf.cuni.cz, ORCID ID: 0000-0003-4698-8379

Martin Štěrba[2], sterbam@lfhk.cuni.cz, ORCID ID: 0000-0003-0145-7697

Tomáš Šimůnek[1], simunekt@faf.cuni.cz, ORCID ID: 0000-0001-5464-4176

Anna Jirkovská[1, $]jirkovan@faf.cuni.cz, ORCID ID: 0000-0002-0131-6010

[1]Charles University, Faculty of Pharmacy in Hradec Kralove, Hradec Králové, Czech Republic

[2]Charles University, Faculty of Medicine in Hradec Kralove, Hradec Králové, Czech Republic

[3]Mustansiriyah University, National Center of Hematology, Baghdad, Iraq

[4]Newcastle University, Biosciences Institute, Newcastle upon Tyne, United Kingdom

[$]Corresponding author

KEYWORDS

anthracyclines, cardiotoxicity, XK469, dexrazoxane, topoisomerase II

ABSTRACT

Anthracyclines, such as doxorubicin (adriamycin), daunorubicin, or epirubicin, rank among the most effective agents in classical anticancer chemotherapy. However, cardiotoxicity remains the main limitation of their clinical use. Topoisomerase IIβ has recently been identified as a plausible target of anthracyclines in cardiomyocytes. We examined the putative topoisomerase IIβ selective agent XK469 as a potential cardioprotective and designed several new analogues. In our experiments, XK469 inhibited both topoisomerase isoforms (α and β) and did not induce topoisomerase II covalent complexes in isolated cardiomyocytes and HL-60, but induced proteasomal degradation of topoisomerase II in these cell types. The cardioprotective potential of XK469 was studied on rat neonatal cardiomyocytes, where dexrazoxane (ICRF-187), the only clinically approved cardioprotective, was effective. Initially, XK469 prevented daunorubicin-induced toxicity and p53 phosphorylation in cardiomyocytes. However, it only partially prevented the phosphorylation of H2AX and did not affect DNA damage measured by Comet Assay. It also did not compromise the daunorubicin antiproliferative effect in HL-60 leukemic cells. When administered to rabbits to evaluate its cardioprotective potential *in vivo*, XK469 failed to prevent the daunorubicin-induced cardiac toxicity in either acute or chronic settings. In the following *in vitro* analysis, we found that prolonged and continuous exposure of rat neonatal cardiomyocytes to XK469 led to significant toxicity. In conclusion, this study provides important evidence on the effects of XK469 and its combination with daunorubicin in clinically relevant doses in cardiomyocytes. Despite its promising characteristics, long-term treatments and *in vivo* experiments have not confirmed its cardioprotective potential.

INTRODUCTION

The incidence of malignant diseases is rapidly increasing. In 2021, 19.3 million new cancer cases were diagnosed worldwide, with the dominant occurrence of breast cancer (11.7 %) (Sung et al. 2021). Although new targeted therapy is widely used, anthracycline antibiotics (ANTs; daunorubicin, doxorubicin, epirubicin) remain an indispensable part of chemotherapeutic protocols for treatment of various solid and hematological malignancies (Jasra and Anampa 2018; Teuffel et al. 2013). The mechanisms of the antineoplastic action of ANTs are complex and were reviewed previously (Gewirtz 1999).

The main limitation of ANTs treatment is represented by cardiotoxicity. Its mechanisms are complex and have not been completely unraveled. Recent studies indicate the essential role of the β isoform of DNA topoisomerase II (TOP2B) in the pathophysiology of ANTs cardiotoxicity (Henriksen 2018; Zhang et al. 2012). Considering the possible role of TOP2B in the regulation of gene expression (Austin et al. 2021), this could eventually manifest in the plethora of effects that ANTs exert on cardiomyocytes.

Type II DNA topoisomerases enable DNA replication and transcription by releasing superhelical tension. The alpha isoform (TOP2A) is expressed only in proliferating cells in the late S phase and peak in the G2-M phase, while TOP2B is expressed throughout the cell cycle in all cells, including quiescent and terminally differentiated cells, such as cardiomyocytes. Furthermore, TOP2B can regulate transcription by implementing double strand breaks in gene promotors (Pommier et al. 2022). The effects of drugs targeting TOP2 differ, depending on the step in TOP2 catalytic cycle they interact with. Generally, inhibitors either stabilize the TOP2-DNA covalent complex leading to DNA double-strand break or interact with the complex leaving DNA strands intact (Nitiss 2009).

There are numerous strategies to prevent or reduce anthracycline-induced cardiotoxicity (Corremans et al. 2019). The primary approach to avoid severe heart damage has been the limitation of the anthracycline cumulative doses, although recent evidence shows that there is no safe anthracycline dose in terms of cardiotoxicity induction (Leger et al. 2015). The only cardioprotective agent approved for clinical use is dexrazoxane (ICRF-187) (EMA 2017). To date, several clinical trials have been conducted confirming dexrazoxane cardioprotective efficiency, safety in various populations, and the pharmacoeconomics of its use (Dewilde et al. 2020; Reichardt et al. 2018). Mechanistically, dexrazoxane was reported to act as a catalytic inhibitor of both TOP2 isoforms (Herman et al. 2014), forming the closed clamp conformation of TOP2 with DNA (Roca et al. 1994). However, a conflicting study suggesting dexrazoxane -induced DNA double-strand breaks also appeared (Deng et al. 2015). Furthermore, speculation has been made about dexrazoxane's induction of secondary malignancies in pediatric cancer patients (Tebbi et al. 2007). Several studies later rejected these findings (Getz et al. 2020; Kim et al. 2019). Hence, TOP2B-targeting specificity could be beneficial in the prevention of anthracycline-induced cardiotoxicity (Jirkovsky et al. 2021).

The compound XK469 (2(R)-[4-(7-chloro-2-quinoxalinyl)oxyphenoxy]propionic acid; NSC698215) was initially reported to act as a selective TOP2B poison (Gao et al. 1999). XK469 inhibited the activity of both TOP2A and TOP2B measured by the DNA relaxation assay, with the IC_{50} for TOP2B significantly lower than for TOP2A. Furthermore, the authors identified XK469-induced protein-DNA crosslinks using a SV40 replicating genomes in solution, and band depletion assay and CsCl gradients in cells (replicating cultures of MCF-7 and African green monkey cells). TOP2B selectivity was further suggested by Snapka et al. (2001) using TOP2B-depleted mouse

embryonic fibroblasts, where $TOP2B^{+/+}$ cells were more sensitive to XK469 than $TOP2B^{-/-}$ with 2.5 times more profound protein-DNA crosslinks. Three clinical studies were conducted to treat advanced solid tumors, advanced neuroblastoma, and refractory hematologic cancer (Alousi et al. 2007; Stock et al. 2008; Undevia et al. 2008). The Phase I pharmacokinetic dose-escalation study showed its long half-life (63 h) that led to relatively high maximal plasmatic concentrations (58-292.3 µg/ml or 158-797 µM, if XK469 Mr = 366.73 g/mol). This study found limited anticancer activity and bone marrow toxicity in higher doses. Furthermore, derivatives of XK469 with 7-substituted quinoxaline showed significant antiproliferative properties that can be attributed to the inhibitory activity of TOP2A (Hazeldine et al. 2001; Hazeldine et al. 2002). We hypothesized that XK469 or some of its analogues could have cardioprotective efficacy. To test this hypothesis, we performed 1) *in vitro* and *in vivo* cardiotoxicity studies using clinically relevant concentrations of daunorubicin, dexrazoxane and XK469, 2) synthesized and evaluated the cardioprotective activity of XK469 analogues, 3) evaluated the biochemical activities of XK469 in our cell models in the clinically relevant concentrations.

MATERIALS AND METHODS

Materials

Daunorubicin and dexrazoxane were purchased as hydrochloric salts (pharmaceutical grade) from Euroasian Chemicals Pvt. Ltd. (Mumbai, India). XK469 was obtained from Merck (Germany) Sigma Aldrich (Product Number X3628). For in vivo experiments sodium salt of XK469 was synthesized at the Department of Organic and Bioorganic Chemistry, Faculty of Pharmacy in Hradec Králové, Charles University. XK469 analogues were prepared as described in Supplementary information (Section 1.1). Collagenase type II (Gibco, Thermofisher Scientific, U.S.A.) and pancreatin (Merck) were utilized for cardiomyocyte isolation. Cardiomyocytes were further cultured in Dulbecco´s modified Eagle´s medium with the nutrient mixture (DMEM/F-12) supplemented with penicillin/streptomycin (500 U/mL; P/S) and sodium pyruvate (Lonza, Belgium), horse serum and fetal bovine serum (FBS) from Merck (Germany). Wild-type HL-60 were kept in RPMI medium (Lonza, Belgium), and CRISPR-modified HL-60 were cultured in IMDM medium (Gibco, Thermofisher Scientific, U.S.A.). Both media types were supplemented with FBS and P/S (Lonza, Belgium). For lactate dehydrogenase assay, nicotinamide adenine dinucleotide (NAD^+) was from Serva (Germany), dimethyl sulfoxide (DMSO), Triton X-100 and dithiothreitol were from Merck, potassium phosphate, Tris-HCl buffer, lactic acid and EDTA were purchased from Penta (Czech Republic). Sytox® green nucleic acid stain was obtained from Invitrogen-Molecular Probes (U.S.A.). 3-(4,5-dimethylthiazol-2-yl)-2,5-difenyltetrazolium-bromide (MTT) was purchased from Merck (Germany). Other common chemicals (organic solvents, buffer components, SDS, agarose) were obtained from Merck (Germany), Penta (Czech Republic), or MP Biomedicals (France).

In vitro toxicity

Cardiomyocyte cell culture. Primary rat neonatal cardiomyocytes were isolated from 1- to 3-day-old Wistar rats. Hearts were extracted, minced, and serially digested with collagenase and pancreatin. The cells were separated from the supernatants by centrifugation (300 × g, room temperature, 5 min), resuspended in DF-10 (DMEM F-12, 4 mM sodium pyruvate, 10 % FBS, 5 % HS, 1 % P/S) and plated in large Petri dishes. Two hours later, cardiac fibroblasts attached to the plastic vessel, whereas cardiomyocytes remained floating in the media. The myocytes were plated on day 0 in 24-well or 96-well dishes (0.8×10^6 myocytes/mL, 0.5 mL/well for 24-well plates or 0.1 mL/well for 96-well plates) in DF-10 to yield an almost confluent layer of beating cardiomyocytes by day 2. At day 3, the medium was changed to serum-free DMEM-F12 and all the subsequent assays were conducted in this medium.

Lactate Dehydrogenase Cytotoxicity Assay. Rat neonatal cardiomyocytes were treated with dexrazoxane or XK469 for 3 h, then daunorubicin was added for another 3 h. After that, the cells were washed and incubated in fresh media for 48 h. The lactate dehydrogenase activity was determined in a kinetic assay in a 96-well plate in a Tecan Infinite 200 M micro-plate spectrophotometer (Tecan, Austria). The initial velocity of the lactate dehydrogenase-catalyzed reaction (2.4 mM NAD^+ and 290 mM sodium lactate in 28 mM Tris buffer of pH 8.8) was determined by measuring the rate of increase in absorbance at 340 nm at 25 °C.

Sytox® Green Cytotoxicity Assay. The cardiomyocytes were incubated in 96-well dishes using 3 different treatment schedules. They were either pre-incubated with XK469 or dexrazoxane for 3 h and then co-incubated with daunorubicin for the next 3 h, followed by 48 h in fresh media (Scheme 1; Fig. 1 and Fig. S2) or continuously

with dexrazoxane, XK469 or their combination 48 h (Scheme 2; Fig. 3). Alternatively, the cells were pre-incubated with dexrazoxane or XK469, co-incubated with daunorubicin for 3 h, following by media change and post-incubated with dexrazoxane or XK469 for 48 h (Scheme 3; Fig. S3). The fluorescence was measured at 3, 6, 8, 24 and 48 h (after addition of the dye at final media change; 3 μM final concentration). The fluorescence was measured at 490 nm excitation and 520 nm emission wavelengths using Tecan Infinite 200 M micro-plate spectrophotometer. To determine the total nucleic acid content per well, all of them were lysed at the end of the experiment (8% Triton X-100) for 1 h, 37 °C. The results are expressed as the percentage of control cells (0.1% DMSO).

MTT Viability Assay. HL-60 (human acute promyelocytic leukemia cell line) obtained from ATCC, was cultured in RPMI media (supplemented with 10 % FBS and 1 % P/S). Cells were plated on 96-well plates at a density of 10,000 cells per well in 100 μL of media for 72 h. After that, 25 μL of 3 mg/mL MTT in PBS was added, and after 3 h, formazan crystals were lysed adding 100 μL of lysis buffer (5 % Triton X-100 and 2.5 % HCl in isopropanol) while overnight shaking. Absorbance was measured at 570 nm, subtracting background (690 nm) and the signal of the cell-free wells. The results are expressed as the percentage of control wells (0.1% DMSO). The individual IC_{50} values of tested compounds were first determined in CalcuSyn 1.1 software (Biosoft, UK). Then, the combination studies were performed with the concentration of daunorubicin corresponding to concentration inducing 50% proliferation decrease (IC_{50}; 15 nM) or according to Chou–Talalay method (Chou and Talalay 1984), where the individual substances and combination mixtures were used at concentrations corresponding to fractions and multiples (1/8; 1/4; 1/2; 1; 2; 4) of their IC_{50} values. Combination indexes were determined using CalcuSyn. HL-60 homozygous mutants ($TOP2B^{-/-}$) and the corresponding wild-type controls ($TOP2B^{+/+}$) prepared using CRISPR-Cas9 technology as described previously (Khazeem et al. 2022; Khazeem et al. 2020) and briefly in Supplementary information (Section 1.2) were incubated in IMDM media (Gibco) supplemented with 10 % FBS, and were processed by the same procedure for the viability assay.

In vivo investigations

Male New Zealand white rabbits (n = 42, 12-15 weeks old, 3.0-3.5 kg, Velaz, Czech Republic) were caged individually under standard conditions. The use of animals was approved by the Animal Welfare Committee of the Faculty of Medicine in Hradec Kralove, Charles University. All non-invasive procedures, including echocardiographic examinations were performed under mild anesthesia (ketamine 30 mg/kg and midazolam 1.25 mg/kg, *i.m*). Pentobarbital (individually titrated *i.v.*) was used for surgical anesthesia for final invasive left ventricular catheterization examination and animal overdose.

A pilot pharmacokinetic experiment was performed with two rabbits for a dosing setup of compound XK469 in rabbits in vivo. Compound XK469 (in the form of sodium salt containing 5 mg/kg XK469 free acid) was dissolved in saline and after filtration (0.22 nm) administered intravenously to the marginal ear vein of rabbits. Plasma concentrations were determined using LC-MS (see Section 1.3 in Supplementary information).

For a pilot study of the potential cardioprotective effects of XK469 against chronic anthracycline cardiotoxicity, 20 rabbits were used in a well-established experimental model (Jirkovsky et al. 2013). The cardiotoxicity was induced by repeated administration of daunorubicin (3 mg/kg, *i.v.*, weekly for 10 weeks, n = 5), while controls received saline in the same schedule (1 mL/kg, n = 5). XK469 was dissolved in saline as described above and

administered *i.v.* at 6 mg/kg (n = 5) alone or 45 min before each daunorubicin administration (to the contralateral ear). The LV systolic function was examined using echocardiography (Vivid 4, 10-MHz probe, GE Healthcare Systems Ultrasound, Hatfield, U.K.) under light anesthesia (ketamine and midazolam). Left parasternal long and short axis view were obtained using 2D-guided M-mode scanning to determine LV internal diameters at end diastole and end systole (LVIDd and LVIDs), interventricular septum (IVS) and LV posterior wall (LVPW) thickness at end diastole along with heart rate. The evaluation was performed from three independent records with at least four cardiac cycles in each record. LV fractional shortening (LV FS), LV volumes at end diastole and systole (LVVd and LVVs), LV ejection fraction (LV EF), stroke volume (SV), cardiac output (CO) and LV mass (LVM) were calculated as described in Section 1.4 in Supplementary information.

Catheterization of the LV via *A. carotis sinistra* was performed at the end of the study under individually titrated pentobarbital anesthesia using a Mikro-Tip pressure catheter (2.3F, Millar Instruments, TX, U.S.A.) connected to Chart 5.4.2 software (ADInstruments, Bella Vista, Australia) for data analysis and calculation of indexes of contraction of the LV (dP/dtmax). The evaluation of maximal and minimal dP/dt were performed after animal stabilization (ca. 15 min) from at least ten consecutive cardiac cycles. Cardiac troponin T (cTnT) concentrations in plasma were determined using the Elecsys Troponin T hs STAT test (Roche Diagnostics, Switzerland) with a detection limit of 3 ng/L.

For the study of XK469 effects on DNA damage response induced in the left ventricular myocardium by single drug dose, 20 rabbits were divided into 4 groups. The animals received the same treatments as above, but the experiment was terminated 6 h after administration of the single dose. This time was used based on previously published data (Kollarova-Brazdova et al. 2021). The heart was excised, washed, and briefly perfused with ice-cold saline to remove blood, and the left ventricle was harvested for analysis of p53 by western blot and p53 target genes by reverse transcription quantitative real-time PCR (RT-qPCR).

Molecular analyses

TOP2 Activity Assay – decatenation: Kinetoplast DNA (kDNA) used as a substrate in the assay was isolated in house from Crithidia fasciculata employing a sucrose cushion centrifugation protocol as described previously (Shapiro et al. 1999). Recombinant human TOP2A and TOP2B (at concentrations that provided complete decatenation of 200 ng of kDNA Inspiralis, U.K.) were incubated with kDNA in a reaction buffer (55 mM Tris-HCl, 135 mM NaCl, 10 mM $MgCl_2$, 5 mM DTT, 0.1 mM EDTA, 1 mM ATP, 100 µg/mL bovine serum albumin; pH 7.5) containing 1 % DMSO (with or without inhibitor) for 30 min at 37 °C in a final volume of 30 µL. Reactions were stopped by addition of gel loading buffer (30 µL; 40 % sucrose, 10 mM EDTA, 0.5 mg/mL bromophenol blue, 100 mM Tris−HCl, pH 8) and put on ice. The samples were electrophoresed on a 1% agarose gel in TAE buffer (40 mM Tris base, 20 mM acetic acid, 1 mM EDTA, pH 8.3) at 3 V/cm. Gels were stained with SYBR Safe (Thermo Fisher Scientific) and visualized using a Chemi Doc MP with post hoc densitometric analysis in Image Lab (BioRad, U.S.A.). The intensity of the fully released minicircles corresponding to complete decatenation was compared to the intensity of the catenated kDNA band of the control (untreated sample; 100 %) present on the same gel. IC_{50} values were calculated using the GraphPad Prism 9 software.

Comet Assay: Single-cell gel electrophoresis was performed according to the previously published protocol (Olive and Banath 2006). Briefly, rat neonatal cardiomyocytes were plated in 24-well plate (0.4×10^6 cells/well), whereas

HL-60 were cultured in 12-well plates (0.5×10^6 cells/well). After the drug treatment, cardiomyocytes were detached by Accutase (150 µL, 15 min, room temperature, gentle agitation; Bio-sera, France) and mixed with 250 µL ice-cold phosphate buffer saline (PBS). HL-60 were spun down, washed, and resuspended in 400 µL of ice-cold PBS. The suspension (20 µL) was mixed with 60 µL of 1% low melting point agarose, mounted onto the microscope slide, and lysed overnight (2.5 M NaCl, 0.1 M EDTA, 100 mM Tris, 1 % Triton-X100, pH 10). The next day, after alkaline unwinding (40 min on ice, 0.3 M NaOH), electrophoresis (300 mA, 14 V) was run for 30 min on ice. After neutralization (0.4 M Tris, pH 7.5, 3 × 5 min) DNA in the minigels was stained with ethidium bromide (0.1 µg/mL), documented (Nikon Eclipse Ti-E, Andor Zyla 5.5, Japan) and analyzed with TriTek CometScore Freeware v1.5 for Windows.

Immunodetection of Ser139 phosphorylated H2AX, TOP2A/B and p53: After treatments, HL-60 cells or neonatal cardiomyocytes were lysed in 2% SDS in 0.1 M Tris-Cl (pH 6.8) and boiled at 90 °C for 10 min. Protein concentrations were assessed by BCA assay. Ten micrograms of total protein were loaded on 12% or 7.5% Bio-Rad TGX Stain-free gels, separated by SDS-PAGE (150 V, Bio-Rad Mini-PROTEAN Tetra Cell) and transferred on the nitrocellulose membrane (Bio-Rad Transblot Turbo). The proteins were detected by mouse anti-γH2AX (1:5,000; ab11174, Abcam, U.K.) and HRP-labelled anti-mouse IgG (1:40,000; A9044 Sigma Aldrich, U.S.A.); rabbit anti-TOP2A/B (1:2,000, ab109524, Abcam, U.K.) and HRP-labelled F(ab')2 goat anti-rabbit IgG (1:10,000, ab6112, Abcam, U.K.); or rabbit anti-p53 [p Ser392] (1:1,000, SI-17, NovusBio, U.S.A.) and mouse anti-rabbit HRP-labelled IgG (1:4,000 HAF0007, R&D Systems, U.S.A.). Acquired chemiluminescent signal was normalized to total protein content. Western blot analysis of p53 levels in left ventricular myocardial samples was performed as described previously (Kollarova-Brazdova et al. 2021). Proteins from left ventricular myocardial samples were separated by SDS–PAGE on TGX Stain-Free precast gels (Bio-Rad, U.S.A.). Immunodetection was performed with a mouse anti-p53 purified primary antibody (1:1,000, BP53-12; Exbio Praha, Czech Republic) and anti-mouse secondary antibody (1:1,000, P0447, Polyclonal Goat Anti-Mouse Immunoglobulin/HRP; DAKO Denmark A/S, Denmark).

TARDIS (trapped in agarose DNA immunostaining): The TARDIS method was performed as described previously (Cowell et al. 2011). Briefly, HL-60 cells and neonatal cardiomyocytes were treated as for the Comet assay, then mounted onto the microscope slide in 1% low melting point agarose and lysed for 30 min in the lysis buffer (10 mM EDTA, 1 % SDS, 20 mM sodium phosphate, pH 6.5) and for 30 min in 1 M NaCl. The next day TOP2 was detected by rabbit anti-TOP2A/B (1:100, ab109524, Abcam, U.K.) in 1% BSA in PBS and goat anti-Rabbit IgG (Alexa Fluor 488, 1:500, ab 150085) in 1% BSA in PBS with counterstaining of nucleoids with Hoechst 33342 (Molecular Probes Invitrogen, U.S.A.). The fluorescent signals were detected on Nikon Eclipse Ti-E with camera Andor Zyla 5.5, and the acquired signal was analyzed by CellProfiler 2.1.1.

Gene expression of p21 (CDKN1A): RT–qPCR was performed as described previously (Kollarova-Brazdova et al. 2021). Total RNA was isolated with TRI Reagent (Merck), reversely transcribed to cDNA with High-Capacity cDNA Reverse Transcription Kit, and qPCR analysis was performed using QuantStudio 7 Flex Real-Time PCR System using TaqMan Fast Universal PCR Master Mix (all from Applied Biosystems, U.S.A.). The analyses were performed using commercial assays (ocCDKN1A_Q1 and ocHPRT1_Q3, Generi Biotech, Czech Republic). The expression of the target gene was normalized to the reference gene (Hprt1) expression. To analyze p21 in cardiomyocytes, cells were detached from plates by Accutase (15 min, room temperature, gentle vortexing, Bio-

sera, France), 0.5×10^6 cells were lysed in the lysis buffer (10 mM Tris HCl, pH 7.4, 0.25 % Igepal CA-630, 150 mM NaCl, 1 % DNAse I) according to Shatzkes et al. (2014). After 5 min incubation at room temperature, the lysis was stopped by incubation at 75 °C for 5 min. The expression of p21 was detected by qPCR using Luna Universal Probe One-Step master mix (New England Biolabs, U.K.) and commercial TaqMan assays (Rn00589996-m1, Applied Biosystems, U.S.A.; rB2M, Generi Biotech, Czech Republic) using QuantStudio 6 Flex Real-Time PCR System.

Data Analysis

Data were acquired from at least three independent experiments and were analyzed using commercially available GraphPad 9 Prism for Windows (GraphPad inc., U.S.A.) and CalcuSyn 1.1 software (Biosoft, UK). Statistical significance was evaluated using ANOVA or ANOVA on Ranks depending on data distribution followed by Holm-Sidak´s or Dunn´s post-hoc test. Details of the individual analyses are specified in the corresponding figure captions.

RESULTS

Screening for toxicity and protection in isolated cardiomyocytes. Initially, the toxicity of daunorubicin and protection with XK469 in neonatal cardiomyocytes were determined using lactate dehydrogenase assay according to scheme 1. Daunorubicin (1.2 µM) induced cell death in approximately 50 % of rat neonatal cardiomyocytes. Preincubation with dexrazoxane significantly reduced daunorubicin cytotoxicity (Fig. 1a). Although XK469 was not toxic, only 30 and 100 µM significantly reduced daunorubicin toxicity (Fig. 1b). These preliminary data indicated that XK469 could potentially serve as a cardioprotective agent, although less efficient than dexrazoxane.

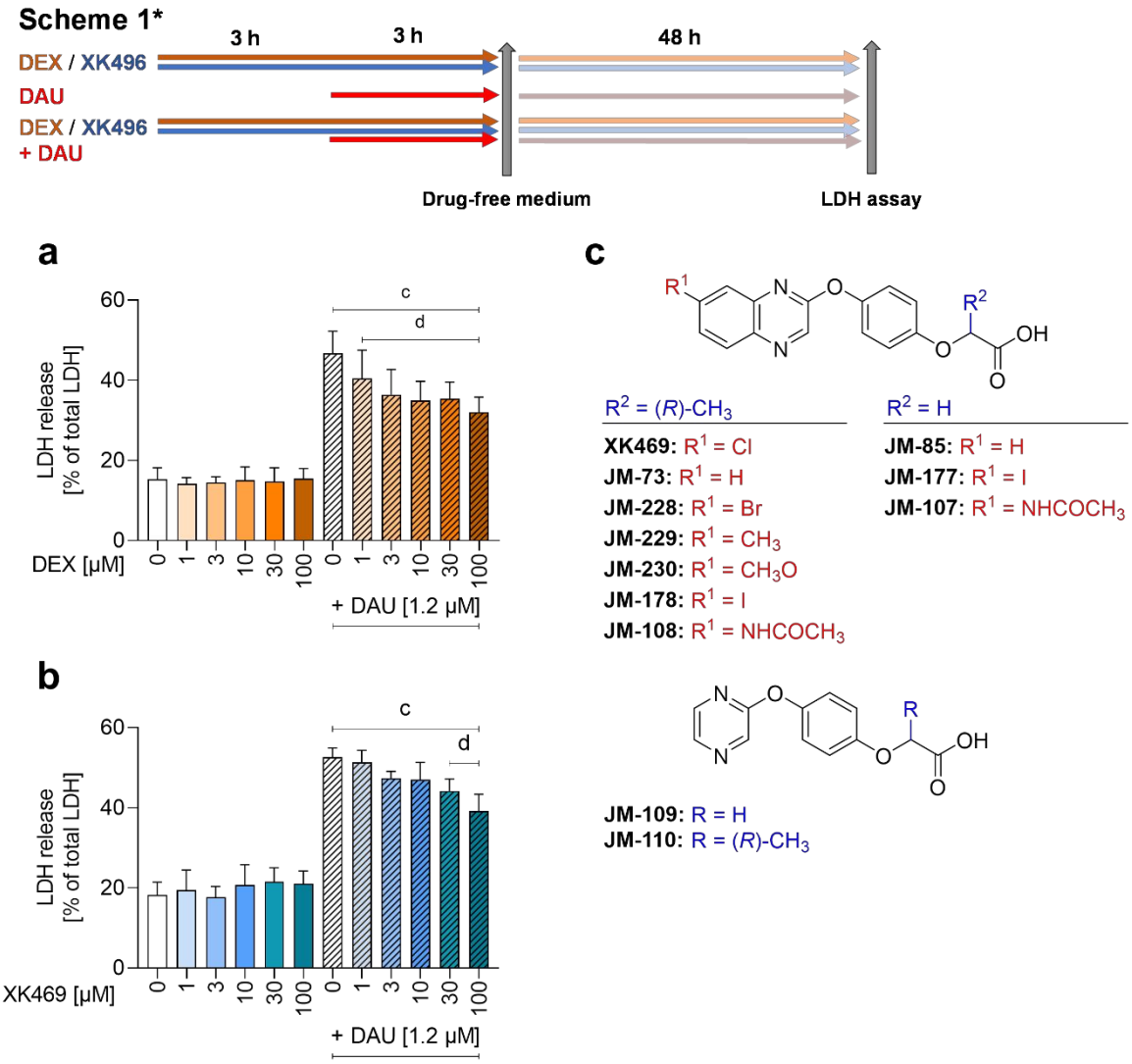

Fig. 1. *Cytotoxicity/protection of dexrazoxane and XK469.* Rat neonatal cardiomyocytes were treated with the range of concentrations of dexrazoxane (DEX) (*a*) and XK469 (*b*) for 3 h either alone or prior to 3 h incubation with 1.2 µM daunorubicin (DAU). After these 6 h, the drug-containing medium was removed, and cells were incubated in fresh media for the next 48 h. Toxicity was assessed by lactate dehydrogenase (LDH) assay. Structure

of XK469 (*c*) and its analogues evaluated in this study. Statistical analyses: n = 4, mean ± SD, One-way ANOVA, Holm-Sidak´s post-hoc test, $P \leq 0.05$, "c" - compared to untreated control cells, "d" - compared to daunorubicin.

As the initial *in vitro* data of XK469 were promising, we decided to explore some of the possible chemical modifications that haven't been reported in the past and we prepared eleven XK469 analogues (Fig. 1c). First, we investigated the role of chlorine substituent in position 7 of the quinoxaline core (compounds JM-73, JM-228, JM-229, JM-230, JM-178 and JM-108). Second, analogues with an acetic acid fragment (JM-85, JM-177 and JM-107) instead of the original propionic acid fragment in XK469 were prepared. Finally, two simplified analogues with a pyrazine core (JM-109, JM-110) were prepared instead of the original quinoxaline. Cytotoxicity and possible protection of synthesized XK469 derivatives against daunorubicin toxicity in neonatal cardiomyocytes were tested using the above-mentioned scheme. Although none of the prepared derivatives was significantly cytotoxic, some of them tended to induce cell death at higher concentrations (JM-178, JM-228). Even though some of the derivatives showed the potential to prevent cardiomyocytes from daunorubicin-induced toxicity (JM-178, JM-228, JM-230), but none was more efficient than XK469 (Fig. S1) Therefore, further studies were performed only with the parent compound.

Antiproliferative effects of XK469, dexrazoxane, and their combinations with daunorubicin. The leukemic cell line HL-60 was incubated with daunorubicin (IC_{50} 15 nM, from pilot experiments) together with dexrazoxane or XK469. Both drugs showed antiproliferative effects themselves (dexrazoxane IC_{50} 9.59 ± 1.94 μM, XK469 IC_{50} 21.64 ± 9.57 μM), and both dexrazoxane and XK469 (from 3 μM onwards) significantly increased the antiproliferative effect of daunorubicin (Fig. 2a, b). More detailed analysis according to Chou and Talalay (1984) to calculate the combination index values, where the HL-60 cells were treated with dexrazoxane or XK469, and their combination with daunorubicin in concentrations corresponding to the fractions and multiples of their IC_{50} (1/8; 1/4; 1/2; 1; 2; 4) showed values around 1, which indicates additive effect of the compounds (Fig. 2c, d).

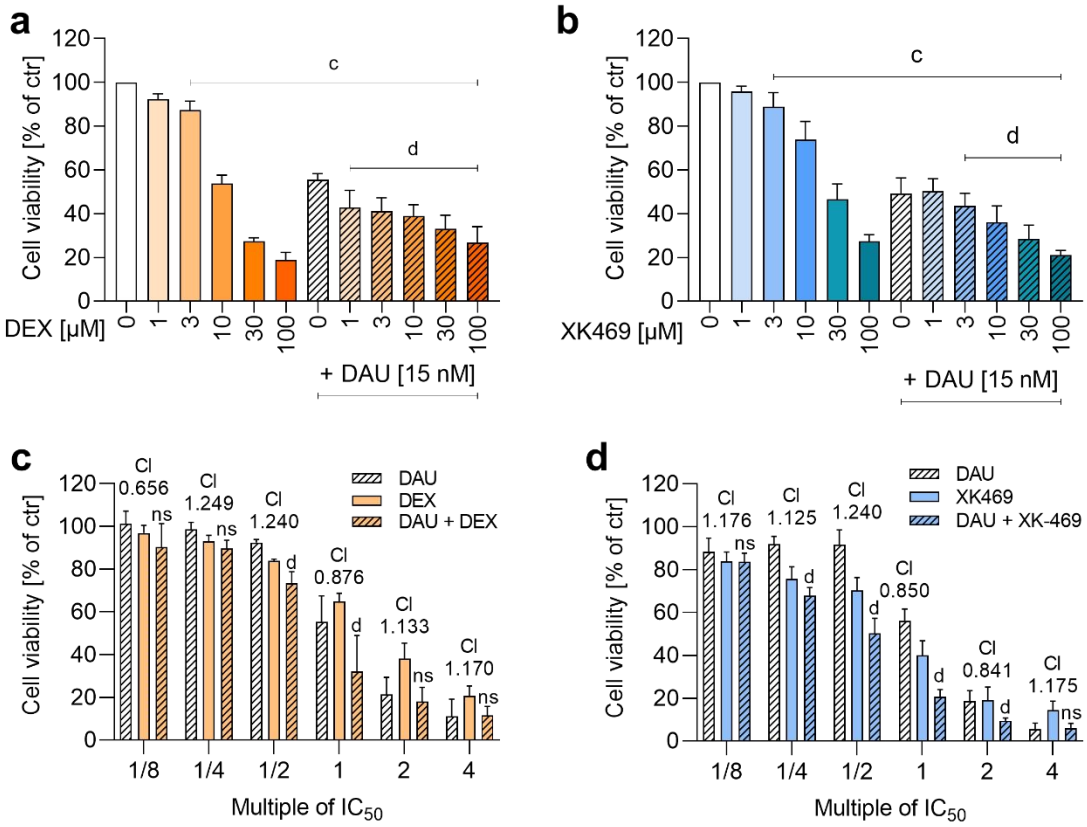

Fig. 2. *Antiproliferative effects of dexrazoxane (DEX) and XK469 and their influence on antiproliferative efficiency of daunorubicin (DAU)*. HL-60 leukemic cells were incubated with increasing concentrations of dexrazoxane (a), or XK469 (b) for 72 h and combined with daunorubicin in its IC_{50} concentration (15 nM). The multiples of the respective IC_{50} values of individual drugs were used in combination experiments according to Chou-Talalay with 48h incubations (c, d; CI – combination index). Toxicity was assessed by MTT assay. Statistical analyses: n = 4, mean ± SD, One-way ANOVA, Holm-Sidak´s post-hoc test, $P \leq 0.05$, "c" - compared to control, "d" - compared to daunorubicin.

Continuous in vitro cytotoxicity/protection studies. As repeated sampling of media for lactate dehydrogenase leakage assay was not possible, the Sytox Green assay was employed for continuous measurements. This gave similar results as lactate dehydrogenase assay in Scheme 1*, but XK469 alone was cytotoxic at higher concentrations (30-100 μM) in every tested time interval (3, 6, 8, 24 and 48 h), and 10 μM was significantly toxic from the 24th hour. Nonetheless, the 3h preincubation with the higher concentrations of XK469 (30-100 μM) afforded similar protection after 48 h as in the lactate dehydrogenase assay (Fig. S2).

In continuous incubations (scheme 2*, "long-term toxicity"), dexrazoxane was non-toxic (Fig. 3a) and all dexrazoxane concentrations protected from the daunorubicin toxicity (Fig. 3b). Toxicity of XK469 increased in a time- and dose-dependent manner, starting at 6 h (100 μM) (Fig. 3c). Its co-incubation with daunorubicin was not significantly protective (Fig. 3d). These data were further supported by scheme 3* treatments, where cardiomyocytes are exposed to dexrazoxane or XK469 for more than 48 h in total (Fig. S3).

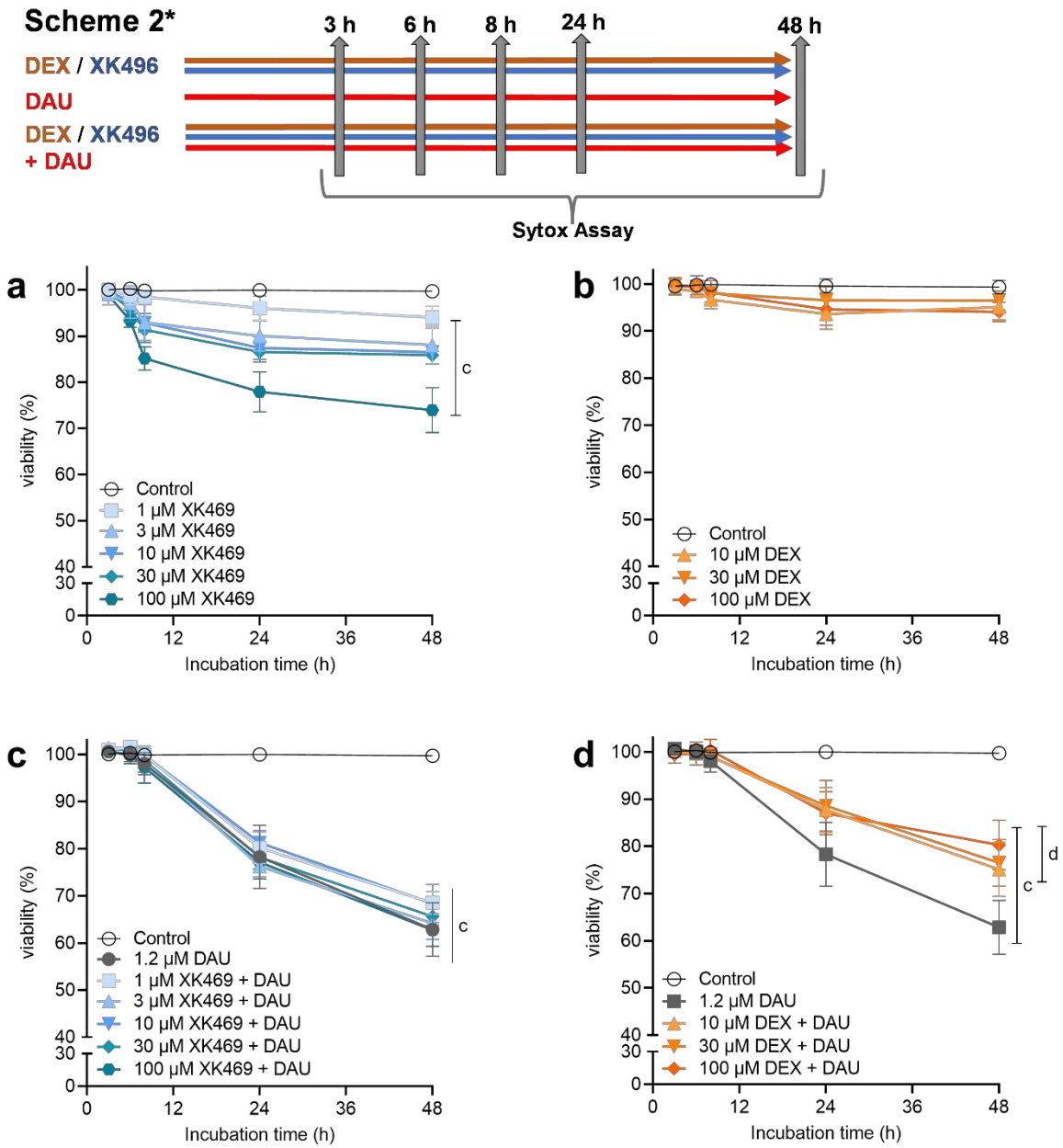

Fig. 3. *Long-term continuous cytotoxicity assessments of dexrazoxane, XK469 and their combinations with daunorubicin in* rat neonatal cardiomyocytes. Cells were incubated with dexrazoxane (a), or XK469 (c) alone or in combinations with daunorubicin (b, d) for up to 48 h. Cytotoxicity was assessed by the Sytox Green. DMSO (0.1 % final concentration) was present in all samples. The statistical analyses: $n \geq 4$, mean ± SD, One-way ANOVA, Dunn's post hoc test, $P \leq 0.05$, "c" – compared to control; "d" – compared to daunorubicin.

TOP2 effects. TOP2 activity was measured using decatenation assay. After the titration of the TOP2 concentration, the enzymes were subjected to dexrazoxane and XK469 (10-1000 µM). No differences were observed between dexrazoxane inhibition of individual TOP2 isoforms (Fig. 4a,c). However, XK469 also inhibited both TOP2

isoforms at comparable IC_{50} values (Fig. 4b,d), which were somewhat higher than in the case of dexrazoxane (XK469 $IC_{50} \approx 130$ µM; dexrazoxane $IC_{50} \approx 60$ µM). Cell-based TARDIS analysis was used to determine dexrazoxane- or XK469-induced TOP2-DNA covalent complexes. The potential for forming these complexes was compared in neonatal cardiomyocytes and HL-60 cells, which differ in levels of TOP2 isoforms and level of differentiation. Etoposide (ETO) was used as a positive control for TOP2-DNA complexes. Dexrazoxane did not cause TOP2-DNA covalent complexes in any cell type or assayed concentration. In XK469, the signal tended to increase in higher concentrations in both cell types, but it did not reach statistical significance (Fig. 4e,f).

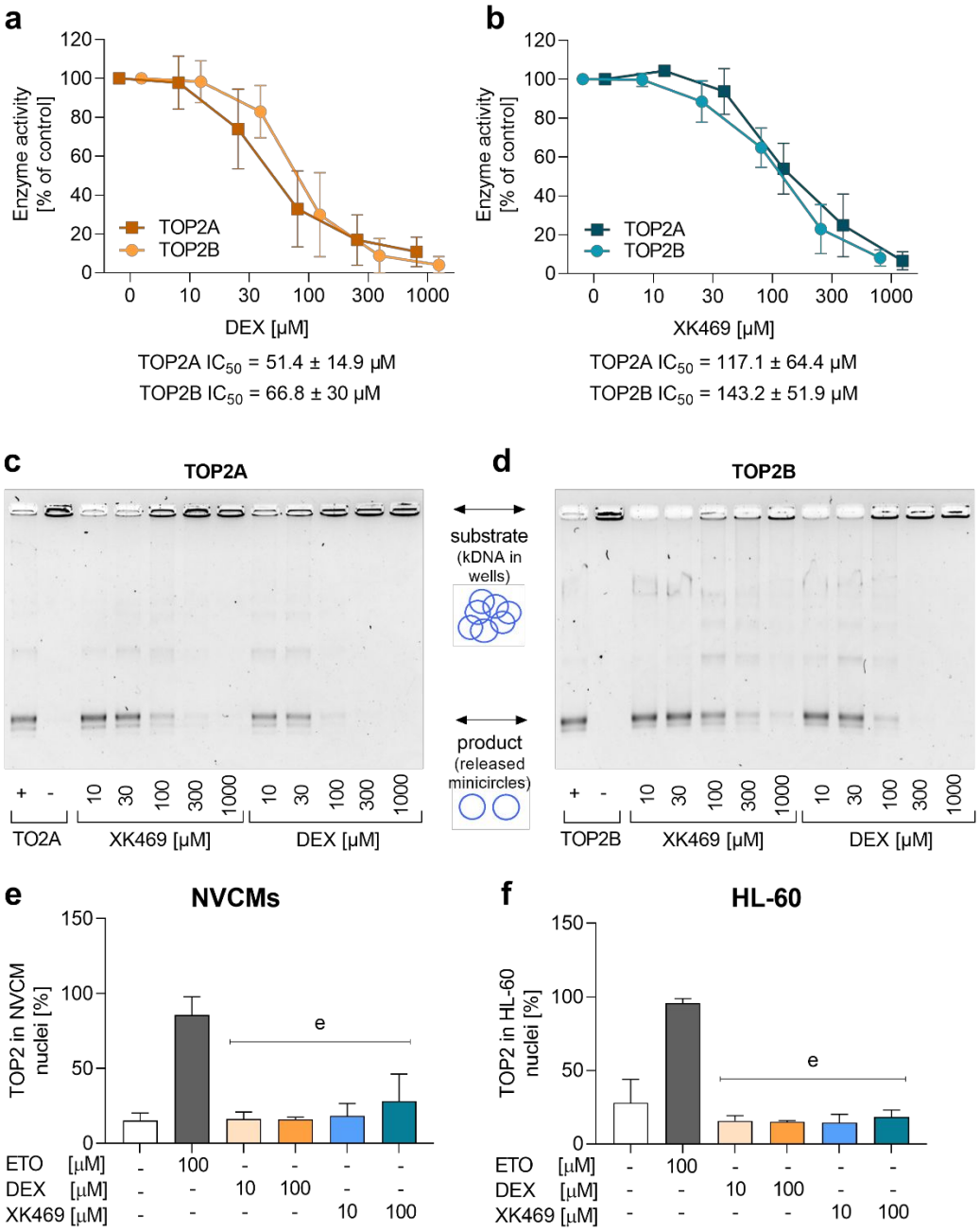

Fig. 4. *TOP2 Assays*. TOP2 activity was analyzed by decatenation assay using purified TOP2 isoforms and catenated DNA. Upper panels show quantification of visualized gels of the inhibition by dexrazoxane (a) and XK469 (b). Lower panels show representative gels of the inhibition of TOP2A (c) and TOP2B (d). TARDIS assay

of TOP2-DNA covalent complexes in neonatal cardiomyocytes (e) and wild-type HL-60 cells (f) were incubated with increasing concentrations of either dexrazoxane or XK469 for 2 h. 100 µM ETO was used as the positive control. Data are expressed as median with an interquartile range of intensities of the individual images. Statistical analyses: n = 4, One-way ANOVA, Holm-Sidak´s post-hoc test, $P \leq 0.05$, "e"-compared to a positive control (100 µM ETO).

We further used HL-60 cells with TOP2B knocked out by CRISPR-Cas9 (Protein expression of both TOP2 isoforms is documented in the supplementary Fig.S10). The activity of both compounds was similar between the wild-type and knockout cells, which indicated the lack of XK469 TOP2 selectivity in HL-60 cells (Fig. 5).

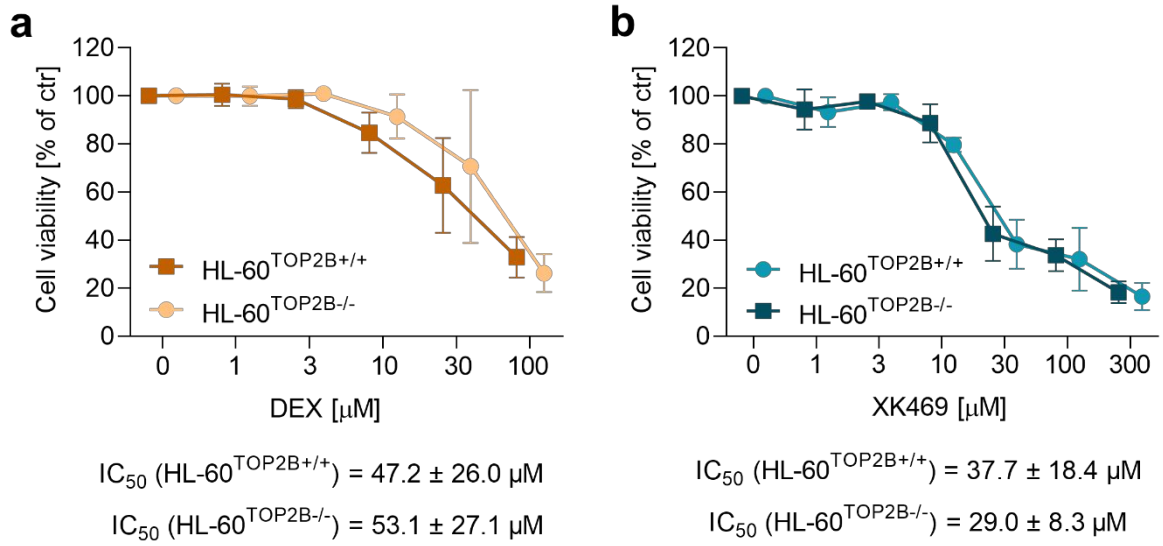

Fig. 5. *Cytotoxicity of dexrazoxane or XK469 in TOP2B$^{+/+}$ and TOP2B$^{-/-}$ in HL-60 cells.* The cells were incubated for 72 h with dexrazoxane (a) and XK469 (b). Statistical analyses: n = 4, mean ± SD, One-way ANOVA, Holm-Sidak´s post-hoc test, $P \leq 0.05$

TOP2 proteasomal degradation in response to its inhibition in cells. The proteasomal degradation of TOP2 by dexrazoxane, first described by Lyu et al. (2007), correlated in our previous studies with cardioprotective activity in isolated cardiomyocytes (Jirkovska et al. 2021; Jirkovsky et al. 2021). In our current study dexrazoxane (10-100 µM) and XK469 (from 3 µM, 30 µM comparable to 10 µM dexrazoxane) induced the degradation of TOP2B in rat neonatal cardiomyocytes after 24 h (Fig. 6).

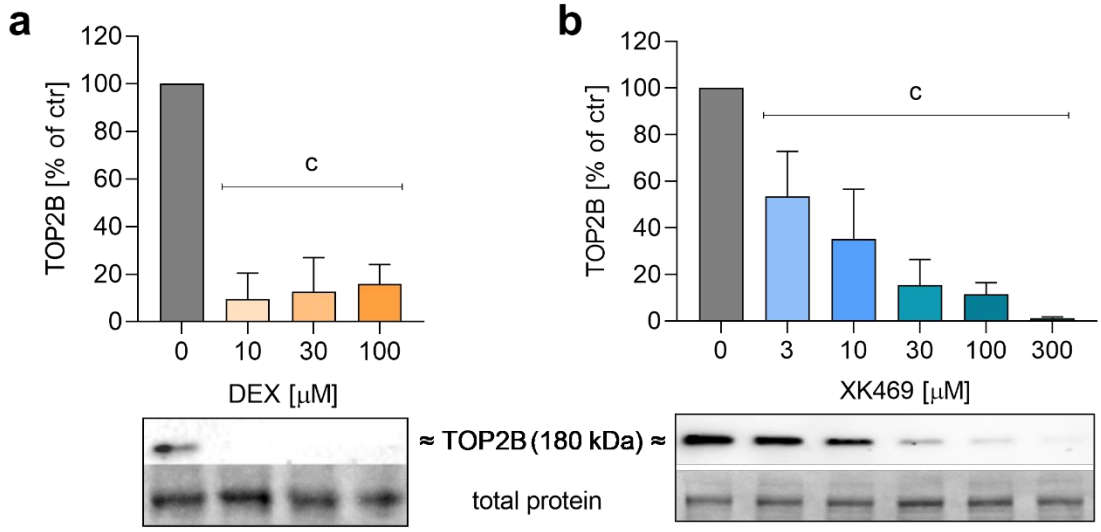

Fig. 6. *TOP2B proteasomal degradation in rat neonatal cardiomyocytes.* Cells were treated with increasing concentrations of dexrazoxane (DEX) (a) or XK469 (b) for 24 h. Then TOP2 content in cells was evaluated by immunodetection. Statistical analyses: n = 3-4, mean ± SD, One-way ANOVA, Holm-Sidak´s post-hoc test, $P \leq 0.05$, "c" compared to drug-free control

DNA damage. Firstly, alkaline Comet Assay was used to detect alkali-labile sites (mostly DNA single- or double-strand breaks, apurinic/apyrimidinic sites). Dexrazoxane did not induce significant damage in neonatal cardiomyocytes, and prevented daunorubicin-induced damage, which correlated with toxicity protection. In contrast, XK469 (100 μM and higher) induced significant Comet Assay signals in neonatal cardiomyocytes. If combined with daunorubicin, XK469 even boosted the damage (Fig. 7e). Phosphorylation of histone γH2AX, one of the first markers of DNA repair initiation, was not increased by dexrazoxane, nor XK469. Moreover, both compounds decreased daunorubicin-induced phosphorylation. (Fig. 7f)

Neither dexrazoxane, (10 μM) nor XK469 (both 10 and 100 μM) induced p53 activation (assessed as the phosphorylation on serine 392) on their own, and both reduced daunorubicin induction in a dose-dependent manner (Fig. 7a, b). The activation of p21 mRNA expression (also known as cyclin-dependent kinase inhibitor 1 and a major target of p53 activity) caused by daunorubicin was significantly decreased by 100 μM dexrazoxane (Fig. 7c). XK469 increased p21 expression similarly to daunorubicin and did not decrease daunorubicin induction (Fig. 7d). This experiment could not be performed in HL-60, as p53 is not expressed in this cell line (Wolf and Rotter 1985).

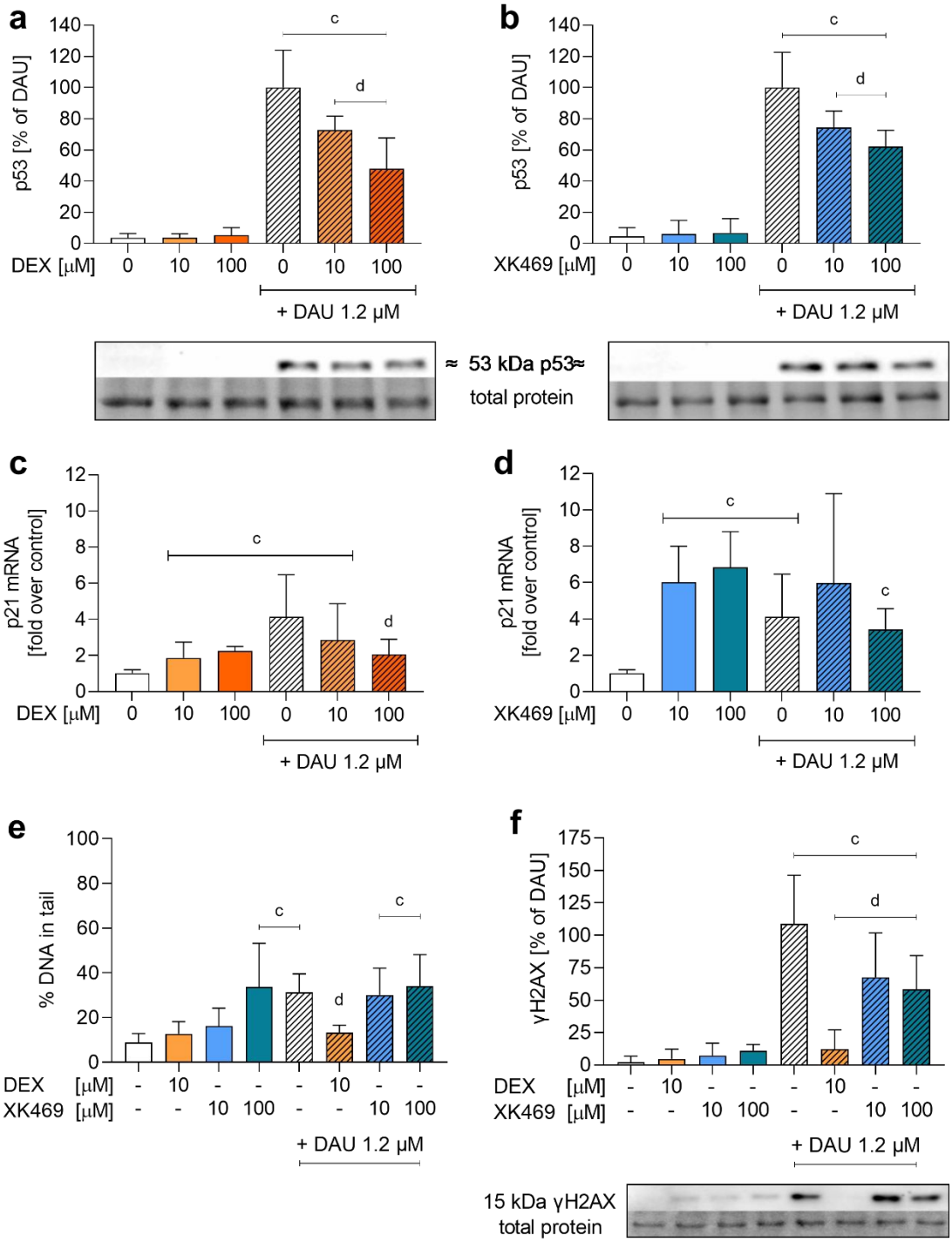

Fig. 7. *Activation of p53 [pSer392], expression of p21 and DNA damage analyses.* Rat neonatal cardiomyocytes were incubated with dexrazoxane (DEX) (orange) and XK469 (blue) either alone or co-incubated with 1.2 μM daunorubicin (DAU). The phosphorylated isoform of p53 protein [pSer392] (a, b), the expression of p21 mRNA (c, d), alkali-labile sites (e) and phosphorylation of γH2AX (f) were evaluated (see Fig. S5-8 for details). Statistical analyses: n = 4, mean ± SD, One-way ANOVA, Holm-Sidak´s post-hoc test, $P \leq 0.05$, "c" - compared to control, "d" - compared to daunorubicin.

In vivo cardioprotection and cardiotoxicity studies of XK469. A pilot pharmacokinetic experiment in two rabbits with 5 mg/kg XK469, *i.v.*, showed maximal plasma concentration (c_{max}) 159 and 177 μM 5 min after drug administration with a relatively slow decline in the elimination phase (8 h post-dose the plasma concentrations were 38 and 42 % of their c_{max}, respectively) (Fig. S4). Based on this data the dose of XK469 for pharmacodynamic investigations was only slightly increased to 6 mg/kg for further *in vivo* experiments. In the initial acute experiments, rabbits were treated with XK469 (6 mg/kg, *i.v.*) alone or 45 min before administration of daunorubicin (3 mg/kg, *i.v.*). After 6 h, p53 at the protein level and p21 at the mRNA level were determined in the left ventricular myocardium. XK469 alone induced neither p53, nor p21 expression in rabbits; nevertheless, it did not decrease p53 or p21 up-regulation induced by daunorubicin (Fig. 8a, b).

In chronic experiments, rabbits were treated with XK469 (6 mg/kg, *i.v.*), daunorubicin (3 mg/kg, *i.v.*) and their combination weekly for 10 weeks. At the end of the experiment, left ventricular systolic function was determined using echocardiography as left ventricular fractional shortening (LVFS) and using left ventricular catheterization as an index of left ventricular contractility (LV dP/dt_{max}), and plasma concentration of cTnT was used as a marker of cardiac damage. XK469 did not ameliorate the daunorubicin-induced worsening of cardiac function/damage parameters. (Fig. 8c-e) Furthermore, other data from echocardiographic examination (Tab. 1) confirm these findings. Daunorubicin induced significant increase in left ventricular internal diameter at end systole (LVIDs) and left ventricular volume at end systole (LVVs), which largely determined significant decrease in LV FS and left ventricular ejection fraction (LV EF), respectively. However, significant changes in the same parameters were also found in the combination group with XK469 and no significant difference between these groups were identified. On the contrary, in our previous study using the identical experimental model, dexrazoxane has been shown to decrease daunorubicin-induced cardiac dysfunction and myocardial damage (Kollarova-Brazdova et al. 2020).

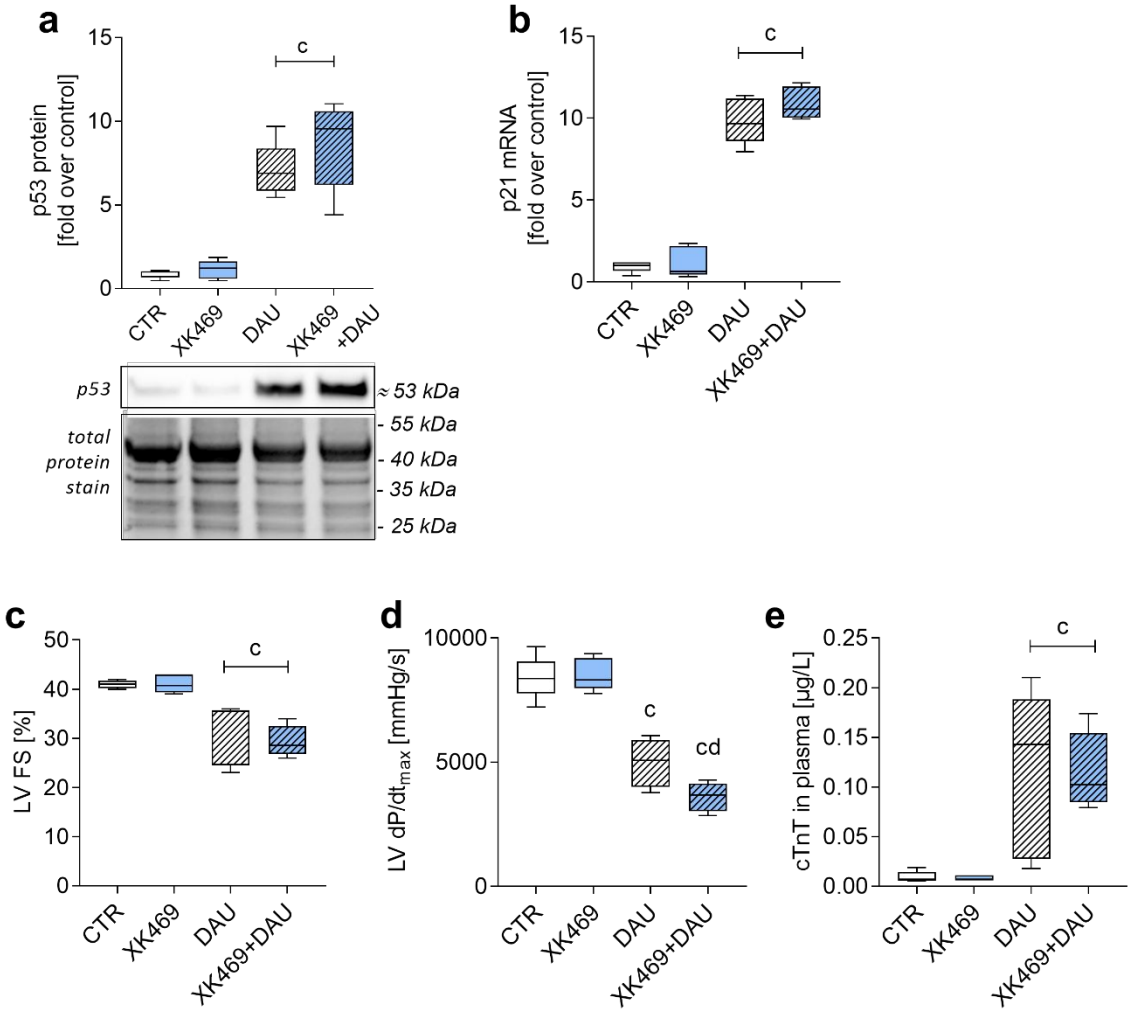

Fig. 8. *Pilot in vivo experiments in rabbits.* In acute experiments (single dose of XK469 (6 mg/kg), daunorubicin (3 mg/kg) and their combination, 6h treatment) the level of p53 protein (a; see Fig. S9 for details) and expression of p21 gene (b) in the left ventricle were evaluated. In chronic settings (10 weekly treatments by XK469 (6 mg/kg), daunorubicin (3 mg/kg), and their combination) left ventricular fractional shortening (LV FS, **c**) and systolic function (LV dP/dt_{max}, d), and cardiac troponin T in plasma (cTnT, e) were evaluated. Statistical analyses: n = 5, mean ± SD, One-way ANOVA, Holm-Sidak´s post-hoc test, $P \leq 0.05$, "c" - compared to control group, "d" - compared to daunorubicin.

Table 1.

Echocardiography examination data

	CTR	XK469	DAU	XK469+DAU
HR (beat/min)	242.7 ± 13.0	251.0 ± 15.6	251.8 ± 18.4	249.8 ± 32.8
LVIDd (cm)	1.71 ± 0.12	1.67 ± 0.16	1.76 ± 0.10	1.77 ± 0.10
LVIDs (cm)	1.01 ± 0.07	0.96 ± 0.09	1.22 ± 0.18 *	1.25 ± 0.10 *
LVFS (%)	40.8 ± 0.6	41.4 ± 1.7	30.6 ± 7.0 *	29.2 ± 3.0 *
LVVd (mL)	8.62 ± 1.54	8.79 ± 1.44	9.19 ± 1.28	9.35 ± 1.27
LVVs (mL)	2.12 ± 0.42	2.04 ± 0.40	3.68 ± 1.52 *	3.75 ± 0.75 *
LVEF (%)	75.4 ± 0.75	76.4 ± 1.2	61.0 ± 11.0 *	59.6± 4.3 *
SV (mL)	6.49 ± 1.12	6.75 ± 1.06	5.51 ± 0.69	5.60 ± 0.75
CO (L/min)	1.57 ± 0.27	1.66 ± 0.18	1.38 ± 0.13	1.44 ± 0.39
IVS (cm)	0.29 ± 0.02	0.28 ± 0.02	0.28 ± 0.03	0.30 ± 0.01
LVPW (cm)	0.26 ± 0.01	0.26 ± 0.01	0.27 ± 0.04	0.28 ± 0.02
LVM (g)	6.13 ± 0.67	5.97 ± 0.67	6.40 ± 1.13	6.88 ± 0.66

Echocardiography examination data obtained by 2D-guided M-mode scanning in parasternal long axis at the tips of mitral valve. HR – heart rate, LVIDd and LVIDs – left ventricular internal diameter at end diastole and end systole, LVFS –fractional shortening, LVVd and LVVs – left ventricular volume at end diastole and end systole (B), LVEF – left ventricular ejection fraction, SV – stroke volume, CO – cardiac output, IVS – interventricular septum thickness at end diastole, LVPW – left ventricular posterior wall thickness at end diastole, LVM – left ventricular mass. CTR – the control group, XK-469 – the group receiving compound XK-469 (6 mg/kg, i.v.) alone, DAU – the group receiving daunorubicin (3 mg/kg, i.v.), XK469+DAU – the combination group receiving compound XK469 (6 mg/kg, i.v.) 45 min before each daunorubicin (3 mg/kg, i.v.) administration. "*" – statistical significance (One-Way ANOVA, $p<0.05$) in comparison with the control group.

DISCUSSION

Dexrazoxane is the only drug approved for primary prevention of anthracycline cardiotoxicity. However, due to the perceived risks of combining dexrazoxane with anthracyclines, clinical guidelines currently restrict the use of dexrazoxane to certain patient populations (EMA 2017). We have identified XK469 as a potential cardioprotective agent due to its selective inhibition of TOP2B (Gao et al. 1999; Snapka et al. 2001), which could be beneficial, especially in the absence of potential interference with anthracycline anticancer efficacy. Although the reported difference between the catalytic inhibitor dexrazoxane and XK469 as a TOP2B poison seemed discouraging, we reasoned that the poisoning effect could be reduced with some chemical modifications. In addition, XK469 had already entered several first-phase clinical trials as an antineoplastic agent (Alousi et al. 2007; Stock et al. 2008; Undevia et al. 2008). One study showed a long half-life (63 h) of XK469 after 360-3200mg/day (30-60 min *i.v.* infusion) resulting in relatively high maximum plasma concentrations (158-797μM XK469) (Undevia et al. 2008).

Based on previous structure-activity relationship reports (Hazeldine et al. 2001; Hazeldine et al. 2002), we prepared several structural analogues of XK469 and compared their cardioprotective effects to dexrazoxane in a protocol (Jirkovska-Vavrova et al. 2015), inspired by its clinical application and previous works by Hasinoff (2002). Neonatal rat cardiomyocytes were used for the in vitro study as a compromise between cardiac origin immortalized cell lines, that all show proliferating phenotype that interferes with the assessment of cardiotoxicity and cardioprotection with dexrazoxane (the results may reflect more the antiproliferative than cardiotoxic effects) and isolated adult cardiomyocytes that are less likely to withstand longer incubations. None of the analogues exhibited superior protection than DEX or XK469 itself (protective from 1 μM, and 30 μM, respectively). Only JM-230, where the chlorine from the original XK469 was changed to bromide, and JM-228, which was substituted with the methoxy group instead of chlorine, showed some protection. The highest dose of JM-230 (300 μM) was less protective than lower doses, indicating potential toxicity. Therefore, we continued further experiments with the original XK469. Due to the different pharmacokinetic parameters between DEX and XK469 and the signs of toxicity in the analogue JM-230, we decided to assess the long-term toxicity using Sytox assay, which allows for repeated measurements. XK469 was significantly toxic after 48 h at all concentrations tested (1-100 μM) and the highest concentrations were toxic even at shorter intervals. Unlike DEX, XK469 did not decrease DAU-induced toxicity.

In previous reported biochemical assays, XK496 exhibited significantly greater inhibition of TOP2B relaxation compared to TOP2A (IC_{50} for TOP2B 160 μM, IC_{50} for TOP2A 5 mM), with preference also in the band depletion assay, and the induction of covalent TOP2-DNA complexes in cells (Gao et al. 1999). We assessed TOP2 activity using both TOP2 isoforms (purchased from Inspiralis, Inc.) using catenated DNA as a substrate. Before the assessment of inhibition, the activity of the isoforms was titrated as recommended by the manufacturer. Both dexrazoxane and XK469 inhibited the activity of both TOP2 isoforms with comparable potencies. The difference of IC_{50} values between the isoforms was lower than 20 %. Discrepancies between our results and published data may reflect different TOP2 enzyme manufacturers, assay types or specific activity of TOP2 preparations.

Previously, mouse embryonic fibroblasts (MEFs) with genetically depleted TOP2B were twice as resistant to XK469 than wild type (IC_{50} = 581 μM vs 175 μM) (Snapka et al. 2001), supporting XK469 selectivity. We used HL-60 cells deleted for TOP2B. These cancer cells were similarly responsive to both dexrazoxane and XK469, regardless of their TOP2B status. Interestingly, the IC_{50} of dexrazoxane on isolated enzyme corresponds with the

IC_{50} in cells, while the IC_{50} of XK469 was significantly higher in the enzyme assay, which might suggest that TOP2 is not the only target of XK469 responsible for its antiproliferative activity, as was also suggested previously (Mensah-Osman et al. 2002). The faster cell division (and expression of TOP2A) could explain the discrepancy between results obtained in fibroblasts and in cancer cells. As the IC_{50} of XK469 was much higher in fibroblasts (like in cardiomyocytes), we may speculate that this would be caused by general cell toxicity.

Proteasomal degradation of TOP2 in response to its inhibition was described previously for dexrazoxane (Lyu et al. 2007), etoposide and ICRF-193 (Zhang et al. 2006), genistein (Azarova et al. 2010) etc. We have previously reported TOP2 degradation following its inhibition by dexrazoxane in rat cardiomyocytes *in vitro* and *in vivo* in rabbits (Jirkovska et al. 2021; Jirkovsky et al. 2021). However, its importance in the mechanism of cardioprotection is a matter of discussion. In our current study, XK469 caused similar TOP2B degradation as dexrazoxane in neonatal cardiomyocytes. In Jirkovská et al. (2021) significant degradation of more than 50 % of TOP2 was achieved with 1μM dexrazoxane after 24 h, which is comparable to 3μM XK469 in this study. We have not previously studied the time-dependent degradation of TOP2 isoforms in HL-60 cells. Hence, we chose a dose that caused a significant decrease of TOP2 in rat neonatal cardiomyocytes but had the smallest effect on proliferation. As we used isoform non-specific antibody in parent HL-60 cells, we were able to follow both TOP2 isoforms in each sample, thanks to the difference in the molecular weight. Contrary to cardiomyocytes, where the expression of TOP2A is negligible (Uhlen et al. 2015), and only a single band corresponding to TOP2B was detected, both isoforms can be detected in HL-60 samples. We used quantification of both isoforms in the parent HL-60 as similar results were obtained with separate quantification. The depletion was not significant until 48 h of incubation with 10 μM dexrazoxane and at no time point with the same concentration of XK469. No significant change was observed also in the $TOP2B^{-/-}$ HL-60 cells with only TOP2A detectable on the membranes.

Previously, XK469 was described to poison TOP2 as measured by filter elution assay of SV-40 TOP2-DNA complexes and band depletion assay in African green monkey cells and genomic TOP2-DNA complexes in MCF-7 cells using supratherapeutic concentrations (1-5 mM) and brief incubation (15 min), which led to trapping of mainly TOP2B, but also some TOP2A (Gao et al. 1999). In the present study, TOP2 poisoning was analyzed by the TARDIS immunostaining method, which has the advantage of TOP2 covalent complexes analysis in individual cells *in situ* (Cowell et al. 2011). Our aim was to assess the possible TOP2 covalent complexes in the clinically relevant doses in post-mitotic cardiomyocytes. Dexrazoxane at concentrations approaching maximal plasma levels (Earhart et al. 1982; Vogel et al. 1987) did not induce TOP2-DNA covalent complexes in either cell type after 2 h of incubation. The same lack of TOP2 covalent complexes was seen with 10 and 100 μM XK469, while clinically relevant concentration of etoposide (Schroeder et al. 2003), used as a positive control, induced a robust signal. Thus, XK469 does not induce TOP2 covalent complexes in doses that effectively induce cardioprotection.

DNA damage was determined by an alkaline comet assay and immunoblotting of γH2AX. The Comet Assay detects the primary DNA double-strand breaks and all so-called alkali-labile sites (apurinic and apyrimidinic sites, phosphotriesters) converted under alkaline conditions to double-strand breaks (Olive and Banath 2006). γH2AX indicates the recruitment of DNA repair factors to the place of DNA lesions, and thereby the initiation of DNA repair pathways (Millan-Zambrano et al. 2022). Dexrazoxane did not induce DNA damage itself and decreased daunorubicin-induced damage in cardiomyocytes, but incubation with XK469 resulted in more complex results. Comet Assay, contrary to γH2AX, detected damage generated by 100 μM XK469 in both neonatal cardiomyocytes

and HL-60, in contrast to the study by Subramanian, where the damage caused by 100 μg/mL XK469 (273 μM) in proliferating HCT-116 cells was not detected (Subramanian et al. 2002). Moreover, preincubation cardiomyocytes with XK469 before daunorubicin did not decrease the Comet Assay signal but decreased γH2AX phosphorylation induced by daunorubicin. Consistently with the literature, we detected increased serine 392 phosphorylation (pSer392) in p53 after anthracycline treatment (Castrogiovanni et al. 2018; Lu et al. 2013). In our study the daunorubicin-induced phosphorylation was prevented by both dexrazoxane and XK469. Substantial activation of p21 was induced by daunorubicin, but also XK469, and their combination. But p21 can also be activated by a p53-independent pathway following DNA damage (Macleod et al. 1995). This would correspond with the results of DNA damage we obtained by Comet Assay, where a DNA lesion that is undetected by γH2AX phosphorylation was probably induced by XK469.

Since in vitro tests showed ambiguous results, we introduced XK469 pre-treatment to our well-established model of chronic anthracycline cardiotoxicity in vivo (Jirkovsky et al. 2021; Kollarova-Brazdova et al. 2020; Simunek et al. 2004). While rats are often used as model animals in anthracycline cardiotoxicity, we have been using rabbits for chronic anthracycline cardiotoxicity studies as they can be repeatedly administered intravenously with anthracyclines and dexrazoxane (or other cardioprotective) in a clinically relevant schedule and the assessment of functional cardiac parameters is more feasible in bigger animal. Moreover, this non-rodent animal exerts more human-like pharmacokinetics and other functional parameters than rats. Finally, we have previously developed both *in vitro* and *in vivo* model with the emphasis on the translatability and clinical relevance regarding the pathological outcomes of anthracycline cardiotoxicity and the cardioprotection by dexrazoxane.

Initial in vitro screening was done using the commercially available (possibly racemic) XK469. But previous studies indicated a preferential activity of R-form of XK469 (Gao et al. 1999), which was thus synthesized for the pilot in vivo experiments. XK469 (6 mg/kg, i.v.) 45 min before daunorubicin (3 mg/kg, i.v.) given weekly for 10 weeks neither diminished the detrimental effects of daunorubicin on left ventricular cardiac function (echocardiography and catheterization) nor it prevented damage of cardiomyocytes (cTnT). Moreover, 6 h after a single administration, XK469 did not decrease the daunorubicin-induced elevation of p53 and p21 expression. In our previous studies, using the same experimental system, dexrazoxane administration (60 mg/kg, i.p.) 30 min before daunorubicin (3 mg/kg, i.v.) protected from all the functional and structural impairments in the chronic settings (Jirkovsky et al. 2013; Kollarova-Brazdova et al. 2020; Simunek et al. 2004). Moreover, a more potent dexrazoxane analogue protected from both chronic and acute impairments mentioned above (Kollarova-Brazdova et al. 2021).

CONCLUSION

XK469 was selected for cardioprotective studies based on its reported TOP2B selectivity. The cardioprotective potential of XK469 or its analogues against anthracycline cardiotoxicity was never evaluated. This article is thus the first assessment of the potential cardioprotective effect of XK469, along with its eleven close analogues, using both *in vitro* and chronic *in vivo* anthracycline cardiotoxicity models. As TOP2 poisoning seemed to be a discouraging feature, we aimed to develop a series of analogues with potentially better properties, although, without the availability of a clear mechanism of inhibition nor the TOP2 binding site, the design could not be rational. No analogue from the series was better in the cardioprotective effectivity, thus all the next analyses were done using the original XK469. The TOP2 isoform selectivity was not confirmed in this study, as well as TOP2 poisoning in clinically relevant concentrations of XK469 in postmitotic cardiomyocytes and HL-60 leukemic cell line. It seems that XK469 generates DNA damage of different kinds than simple DNA double-strand breaks, which would be expected after TOP2 poisoning. Although the pilot data from cardioprotective studies were promising, the long-term toxicity of XK469 was found to dominate over its potential cardioprotective properties. The prevention of DNA damage in cardiomyocytes seems to be an essential premise for cardioprotection, which was obvious in acute and chronic in vivo experiments in rabbits. Therefore, while this study provides new information about XK469, despite its promising characteristics, long-term cardiomyocyte treatments and *in vivo* experiments did not confirm its cardioprotective potential.

STATEMENTS AND DECLARATIONS

Funding. This study was supported by the Czech Science Foundation (project 21-16195S), Charles University (projects GAUK 1674119 and SVV 260664), and by project InoMed reg. No. CZ.02.1.01/0.0/0.0/18_069/0010046: Pre-application research into innovative medicines and medical technologies project co-funded by the European Regional Development Fund.

Conflict of interest. The authors have no relevant financial or non-financial interests to disclose.

Author contributions. All authors contributed to the study conception and design. Material preparation, data collection and analysis were performed by Veronika Keresteš, Jan Kubeš, Lenka Applová, Petra Kollárová, Olga Lenčová-Popelová, Iuliia Melnikova, Galina Karabanovich, and Hana Bavlovič Piskáčková. The first draft of the manuscript was written by Veronika Keresteš and all authors commented on previous versions of the manuscript. All authors read and approved the final manuscript.

Data availability. The datasets generated during and/or analyzed during the current study are available from the corresponding author on reasonable request.

REFERENCES

Alousi AM, Boinpally R, Wiegand R, Parchment R, Gadgeel S, Heilbrun LK, Wozniak AJ, DeLuca P, LoRusso PM. 2007. A phase 1 trial of xk469: Toxicity profile of a selective topoisomerase ii beta inhibitor. Investigational New Drugs. 25(2):147-154.

Austin CA, Cowell IG, Khazeem MM, Lok D, Ng HT. 2021. Top2b's contributions to transcription. Biochem Soc T. 49(6):2483-2493.

Azarova AM, Lin RK, Tsai YC, Liu LF, Lin CP, Lyu YL. 2010. Genistein induces topoisomerase iibeta- and proteasome-mediated DNA sequence rearrangements: Implications in infant leukemia. Biochemical and biophysical research communications. 399(1):66-71.

Castrogiovanni C, Waterschoot B, De Backer O, Dumont P. 2018. Serine 392 phosphorylation modulates p53 mitochondrial translocation and transcription-independent apoptosis. Cell death and differentiation. 25(1):190-203.

Corremans R, Adao R, De Keulenaer GW, Leite-Moreira AF, Bras-Silva C. 2019. Update on pathophysiology and preventive strategies of anthracycline-induced cardiotoxicity. Clin Exp Pharmacol Physiol. 46(3):204-215.

Cowell IG, Tilby MJ, Austin CA. 2011. An overview of the visualisation and quantitation of low and high mw DNA adducts using the trapped in agarose DNA immunostaining (tardis) assay. Mutagenesis. 26(2):253-260.

Deng S, Yan T, Nikolova T, Fuhrmann D, Nemecek A, Godtel-Armbrust U, Kaina B, Wojnowski L. 2015. The catalytic topoisomerase ii inhibitor dexrazoxane induces DNA breaks, atf3 and the DNA damage response in cancer cells. British journal of pharmacology. 172(9):2246-2257.

Dewilde S, Carroll K, Nivelle E, Sawyer J. 2020. Evaluation of the cost-effectiveness of dexrazoxane for the prevention of anthracycline-related cardiotoxicity in children with sarcoma and haematologic malignancies: A european perspective. Cost Eff Resour Alloc. 18:7.

Earhart RH, Tutsch KD, Koeller JM, Rodriguez R, Robins HI, Vogel CL, Davis HL, Tormey DC. 1982. Pharmacokinetics of (+)-1,2-di(3,5-dioxopiperazin-1-yl)propane intravenous infusions in adult cancer patients. Cancer research. 42(12):5255-5261.

Questions and answers on cardioxane (dexrazoxane, powder for solution for injection, 500 mg). 2017. [accessed]. http://www.ema.europa.eu/ema/index.jsp?curl=pages/medicines/human/referrals/Dexrazoxane/

human_referral_.

Gao H, Huang KC, Yamasaki EF, Chan KK, Chohan L, Snapka RM. 1999. Xk469, a selective topoisomerase iibeta poison. Proceedings of the National Academy of Sciences of the United States of America. 96(21):12168-12173.

Getz KD, Sung L, Alonzo TA, Leger KJ, Gerbing RB, Pollard JA, Cooper T, Kolb EA, Gamis AS, Ky B, Aplenc R. 2020. Effect of dexrazoxane on left ventricular systolic function and treatment outcomes in patients with acute myeloid leukemia: A report from the children's oncology group. Journal of clinical oncology : official journal of the American Society of Clinical Oncology. 38(21):2398-2406.

Gewirtz DA. 1999. A critical evaluation of the mechanisms of action proposed for the antitumor effects of the anthracycline antibiotics adriamycin and daunorubicin. Biochemical pharmacology. 57(7):727-741.

Hasinoff BB. 2002. Dexrazoxane (icrf-187) protects cardiac myocytes against hypoxia-reoxygenation damage. Cardiovascular toxicology. 2(2):111-118.

Hazeldine ST, Polin L, Kushner J, Paluch J, White K, Edelstein M, Palomino E, Corbett TH, Horwitz JP. 2001. Design, synthesis, and biological evaluation of analogues of the antitumor agent, 2-{4-[(7-chloro-2-quinoxalinyl)oxy]phenoxy}propionic acid (xk469). Journal of medicinal chemistry. 44(11):1758-1776.

Hazeldine ST, Polin L, Kushner J, White K, Bouregeois NM, Crantz B, Palomino E, Corbett TH, Horwitz JP. 2002. Synthesis and biological evaluation of some bioisosteres and congeners of the antitumor agent, 2-{4-[(7-chloro-2-quinoxalinyl)oxy]phenoxy}propionic acid (xk469). Journal of medicinal chemistry. 45(14):3130-3137.

Henriksen PA. 2018. Anthracycline cardiotoxicity: An update on mechanisms, monitoring and prevention. Heart. 104(12):971-977.

Herman EH, Hasinoff BB, Steiner R, Lipshultz SE. 2014. A review of the preclinical development of dexrazoxane. Progress in Pediatric Cardiology. 36(1-2):33-38.

Chou TC, Talalay P. 1984. Quantitative analysis of dose-effect relationships: The combined effects of multiple drugs or enzyme inhibitors. Advances in enzyme regulation. 22:27-55.

Jasra S, Anampa J. 2018. Anthracycline use for early stage breast cancer in the modern era: A review. Curr Treat Option On. 19(6).

Jirkovska-Vavrova A, Roh J, Lencova-Popelova O, Jirkovsky E, Hruskova K, Potuckova-Mackova E, Jansova H, Haskova P, Martinkova P, Eisner T et al. 2015. Synthesis and analysis of novel analogues of dexrazoxane and its open-ring hydrolysis product for protection against anthracycline cardiotoxicity in vitro and in vivo. Toxicol Res-Uk. 4(4):1098-1114.

Jirkovska A, Karabanovich G, Kubes J, Skalicka V, Melnikova I, Korabecny J, Kucera T, Jirkovsky E, Novakova L, Piskackova HB et al. 2021. Structure-activity relationship study of dexrazoxane analogues reveals icrf-193 as the most potent bisdioxopiperazine against anthracycline toxicity to cardiomyocytes due to its strong topoisomerase ii beta interactions. Journal of medicinal chemistry. 64(7):3997-4019.

Jirkovsky E, Jirkovska A, Bavlovic-Piskackova H, Skalicka V, Pokorna Z, Karabanovich G, Kollarova-Brazdova P, Kubes J, Lencova-Popelova O, Mazurova Y et al. 2021. Clinically translatable prevention of anthracycline cardiotoxicity by dexrazoxane is mediated by topoisomerase ii beta and not metal chelation. Circ Heart Fail. 14(11):e008209.

Jirkovsky E, Lencova-Popelova O, Hroch M, Adamcova M, Mazurova Y, Vavrova J, Micuda S, Simunek T, Gersl V, Sterba M. 2013. Early and delayed cardioprotective intervention with dexrazoxane each show different potential for prevention of chronic anthracycline cardiotoxicity in rabbits. Toxicology. 311(3):191-204.

Khazeem MM, Casement JW, Schlossmacher G, Kenneth NS, Sumbung NK, Chan JYT, McGow JF, Cowell IG, Austin CA. 2022. Top2b is required to maintain the adrenergic neural phenotype and for atra-induced differentiation of sh-sy5y neuroblastoma cells. Mol Neurobiol. 59(10):5987-6008.

Khazeem MM, Cowell IG, Harkin LF, Casement JW, Austin CA. 2020. Transcription of carbonyl reductase 1 is regulated by DNA topoisomerase ii beta. FEBS letters. 594(20):3395-3405.

Kim H, Kang HJ, Park KD, Koh KN, Im HJ, Seo JJ, Lee JW, Chung NG, Cho B, Kim HK et al. 2019. Risk factor analysis for secondary malignancy in dexrazoxane-treated pediatric cancer patients. Cancer Res Treat. 51(1):357-367.

Kollarova-Brazdova P, Jirkovska A, Karabanovich G, Pokorna Z, Piskackova HB, Jirkovsky E, Kubes J, Lencova-Popelova O, Mazurova Y, Adamcova M et al. 2020. Investigation of structure-activity relationships of dexrazoxane analogs reveals topoisomerase ii beta

interaction as a prerequisite for effective protection against anthracycline cardiotoxicity. Journal of Pharmacology and Experimental Therapeutics. 373(3):402-415.

Kollarova-Brazdova P, Lencova-Popelova O, Karabanovich G, Kocurova-Lengvarska J, Kubes J, Vanova N, Mazurova Y, Adamcova M, Jirkovska A, Holeckova M et al. 2021. Prodrug of icrf-193 provides promising protective effects against chronic anthracycline cardiotoxicity in a rabbit model in vivo. Clin Sci (Lond). 135(15):1897-1914.

Leger K, Slone T, Lemler M, Leonard D, Cochran C, Bowman WP, Bashore L, Winick N. 2015. Subclinical cardiotoxicity in childhood cancer survivors exposed to very low dose anthracycline therapy. Pediatr Blood Cancer. 62(1):123-127.

Lu Y, Xu D, Zhou J, Ma Y, Jiang Y, Zeng W, Dai W. 2013. Differential responses to genotoxic agents between induced pluripotent stem cells and tumor cell lines. J Hematol Oncol. 6(1):71.

Lyu YL, Kerrigan JE, Lin CP, Azarova AM, Tsai YC, Ban Y, Liu LF. 2007. Topoisomerase iibeta mediated DNA double-strand breaks: Implications in doxorubicin cardiotoxicity and prevention by dexrazoxane. Cancer research. 67(18):8839-8846.

Macleod KF, Sherry N, Hannon G, Beach D, Tokino T, Kinzler K, Vogelstein B, Jacks T. 1995. P53-dependent and independent expression of p21 during cell growth, differentiation, and DNA damage. Gene Dev. 9(8):935-944.

Mensah-Osman EJ, Al-Katib AM, Dandashi MH, Mohammad RM. 2002. 2-[4-(7-chloro-2-quinoxalinyloxy)phenoxy]-propionic acid (xk469) inhibition of topoisomerase ii beta is not sufficient for therapeutic response in human waldenstrom's macroglobulinemia xenograft model. Mol Cancer Ther. 1(14):1315-1320.

Millan-Zambrano G, Burton A, Bannister AJ, Schneider R. 2022. Histone post-translational modifications - cause and consequence of genome function. Nat Rev Genet. 23(9):563-580.

Nitiss JL. 2009. Targeting DNA topoisomerase ii in cancer chemotherapy. Nature reviews Cancer. 9(5):338-350.

Olive PL, Banath JP. 2006. The comet assay: A method to measure DNA damage in individual cells. Nature protocols. 1(1):23-29.

Pommier Y, Nussenzweig A, Takeda S, Austin C. 2022. Human topoisomerases and their roles in genome stability and organization. Nature reviews Molecular cell biology. 23(6):407-427.

Reichardt P, Tabone MD, Mora J, Morland B, Jones RL. 2018. Risk-benefit of dexrazoxane for preventing anthracycline-related cardiotoxicity: Re-evaluating the european labeling. Future Oncol. 14(25):2663-2676.

Roca J, Ishida R, Berger JM, Andoh T, Wang JC. 1994. Antitumor bisdioxopiperazines inhibit yeast DNA topoisomerase ii by trapping the enzyme in the form of a closed protein clamp. Proceedings of the National Academy of Sciences of the United States of America. 91(5):1781-1785.

Shapiro TA, Klein VA, Englund PT. 1999. Isolation of kinetoplast DNA. Methods in molecular biology. 94:61-67.

Shatzkes K, Teferedegne B, Murata H. 2014. A simple, inexpensive method for preparing cell lysates suitable for downstream reverse transcription quantitative pcr. Sci Rep. 4:4659.

Schroeder PE, Jensen PB, Sehested M, Hofland KF, Langer SW, Hasinoff BB. 2003. Metabolism of dexrazoxane (icrf-187) used as a rescue agent in cancer patients treated with high-dose etoposide. Cancer chemotherapy and pharmacology. 52(2):167-174.

Simunek T, Klimtova I, Kaplanova J, Mazurova Y, Adamcova M, Sterba M, Hrdina R, Gersl V. 2004. Rabbit model for in vivo study of anthracycline-induced heart failure and for the evaluation of protective agents. European journal of heart failure. 6(4):377-387.

Snapka RM, Gao H, Grabowski DR, Brill D, Chan KK, Li L, Li GC, Ganapathi R. 2001. Cytotoxic mechanism of xk469: Resistance of topoisomerase iibeta knockout cells and inhibition of topoisomerase i. Biochemical and biophysical research communications. 280(4):1155-1160.

Stock W, Undevia SD, Bivins C, Ravandi F, Odenike O, Faderl S, Rich E, Borthakur G, Godley L, Verstovsek S et al. 2008. A phase i and pharmacokinetic study of xk469r (nsc 698215), a quinoxaline phenoxypropionic acid derivative, in patients with refractory acute leukemia. Investigational New Drugs. 26(4):331-338.

Subramanian B, Nakeff A, Media J, Wentland M, Valeriote F. 2002. Cellular drug action profile paradigm applied to xk469. J Exp Ther Oncol. 2(5):253-263.

Sung H, Ferlay J, Siegel RL, Laversanne M, Soerjomataram I, Jemal A, Bray F. 2021. Global cancer statistics 2020: Globocan estimates of incidence and mortality worldwide for 36 cancers in 185 countries. Ca-Cancer J Clin. 71(3):209-249.

Tebbi CK, London WB, Friedman D, Villaluna D, De Alarcon PA, Constine LS, Mendenhall NP, Sposto R, Chauvenet A, Schwartz CL. 2007. Dexrazoxane-associated risk for acute myeloid leukemia/myelodysplastic syndrome and other secondary malignancies in pediatric hodgkin's disease. Journal of clinical oncology : official journal of the American Society of Clinical Oncology. 25(5):493-500.

Teuffel O, Leibundgut K, Lehrnbecher T, Alonzo TA, Beyene J, Sung L. 2013. Anthracyclines during induction therapy in acute myeloid leukaemia: A systematic review and meta-analysis. British journal of haematology. 161(2):192-203.

Uhlen M, Fagerberg L, Hallstrom BM, Lindskog C, Oksvold P, Mardinoglu A, Sivertsson A, Kampf C, Sjostedt E, Asplund A et al. 2015. Proteomics. Tissue-based map of the human proteome. Science. 347(6220):1260419.

Undevia SD, Innocenti F, Ramirez J, House L, Desai AA, Skoog LA, Singh DA, Karrison T, Kindler HL, Ratain MJ. 2008. A phase i and pharmacokinetic study of the quinoxaline antitumour agent r(+)xk469 in patients with advanced solid tumours. European journal of cancer. 44(12):1684-1692.

Vogel CL, Gorowski E, Davila E, Eisenberger M, Kosinski J, Agarwal RP, Savaraj N. 1987. Phase i clinical trial and pharmacokinetics of weekly icrf-187 (nsc 169780) infusion in patients with solid tumors. Invest New Drug. 5(2):187-198.

Wolf D, Rotter V. 1985. Major deletions in the gene encoding the p53 tumor antigen cause lack of p53 expression in hl-60 cells. Proceedings of the National Academy of Sciences of the United States of America. 82(3):790-794.

Zhang A, Lyu YL, Lin CP, Zhou N, Azarova AM, Wood LM, Liu LF. 2006. A protease pathway for the repair of topoisomerase ii-DNA covalent complexes. The Journal of biological chemistry. 281(47):35997-36003.

Zhang S, Liu X, Bawa-Khalfe T, Lu LS, Lyu YL, Liu LF, Yeh ET. 2012. Identification of the molecular basis of doxorubicin-induced cardiotoxicity. Nature medicine. 18(11):1639-1642.

SUPPLEMENTARY INFORMATION

Exploring the effects of topoisomerase II inhibitor XK469 on anthracycline cardiotoxicity and DNA damage: insights from *in vitro* and *in vivo* studies

Charles University, Faculty of Pharmacy in Hradec Králové, Heyrovského 1203, 500 05 Hradec Králové, Czech Republic.

Veronika Keresteš[1], Jan Kubeš[1], Lenka Applová[1], Petra Kollárová[2], Olga Lenčová-Popelová[2], Iullia Melnikova[1], Galina Karabanovich[1], Mushtaq M. Khazeem[3], Hana Bavlovič Piskáčková[1], Petra Štěrbová-Kovaříková[1], Caroline A. Austin[4], Jaroslav Roh[1], Martin Štěrba[2], Tomáš Šimůnek[1], Anna Jirkovská[1], $

$Corresponding author

Charles University, Faculty of Pharmacy[1] and Faculty of Medicine[2] in Hradec Kralove, Czech Republic

[3]Mustansiriyah University, National Center of Hematology, Iraq

[4]Newcastle University, Biosciences Institute, United Kingdom

Email: jirkovan@faf.cuni.cz

1 SUPPLEMENTAL METHODS AND MATERIALS

1.1 Chemistry

General. The structural identities of the prepared compounds were confirmed by ^{1}H-NMR and ^{13}C-NMR spectroscopy. Each of the prepared compounds had ≥95% purity, as determined using elemental analysis. All chemicals used for synthesis were obtained from Merck (Germany) and were used as received. TLC was performed on Merck aluminum plates with silica gel 60 F_{254}. Merck Kieselgel 60 (0.040-0.063 mm) was used for column chromatography. Melting points were recorded with a Büchi B-545 apparatus (BUCHI Labortechnik AG, Flawil, Switzerland) and are uncorrected. ^{1}H and ^{13}C NMR spectra were recorded using a Varian Mercury VNMR S500 NMR spectrometer or Jeol JNM-ECZ600R. Chemical shifts were reported as δ values in parts per million (ppm) and were indirectly referenced to tetramethylsilane (TMS) via the solvent signal. The elemental analysis was carried out on an Automatic Microanalyser EA1110CE (Fisons Instruments S.p.A., Milano, Italy).

Synthesis of 3-chloroquinoxalin-6-amine (4)

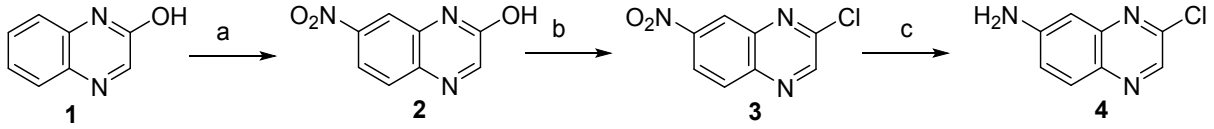

(a) A solution of 65% nitric acid (3.3 g/2.4 mL, 34 mmol) in acetic acid (10 mL) was added dropwise to solution of quinoxalin-2-ol (**1**) (5.0 g, 34 mmol) in acetic acid (40 mL). The reaction mixture was stirred at room temperature for 18 h. The formed precipitation was filtered off, the filtrate cake was washed with water to neutral pH and dried over P_2O_5. 7-Nitroquinoxalin-2-ol (**2**) was obtained in 83% yield as a light-yellow solid; mp 277-279 °C (lit mp (Deng et al. 2011) 273-276 °C). ^{1}H NMR (600 MHz, DMSO) δ 12.69 (s, 1H), 8.31 (s, 1H), 8.06 (d, J = 2.5 Hz, 1H), 8.03 (dd, J = 2.5, 8.8 Hz, 1H), 7.97 (d, J = 8.8 Hz, 1H). ^{13}C NMR (151 MHz, DMSO) δ 156.07, 155.08, 148.14, 135.84, 132.88, 130.76, 118.00, 111.74. Elem. Anal. Calcd. for $C_8H_5N_3O_3$: C, 50.27; H, 2.64; N 21.98. Found: C, 50.57; H 2.61; N 21.83.

(b) 7-Nitroquinoxalin-2-ol (**2**) (4.9 g, 25 mmol) was dissolved in $POCl_3$ (40 mL) and DMF (0.1 mL) was added. The reaction mixture was stirred for 3 h at 110 °C and after cooling poured into ice. The formed precipitation was filtered off, the filtrate cake was washed with water to neutral pH and dried over P_2O_5. 2-Chloro-7-nitroquinoxaline (**3**) was obtained in 94% yield as a light-yellow solid; mp 184-186 °C (lit mp (Deng et al. 2011) 185-189 °C). ^{1}H NMR (600 MHz, DMSO) δ 9.17 (s, 1H), 8.82 (d, J = 2.5 Hz, 1H), 8.54 (dd, J = 2.5, 9.1 Hz, 1H), 8.35 (d, J = 9.1 Hz, 1H). ^{13}C NMR (151 MHz, DMSO) δ 149.79, 149.45, 148.90, 143.45, 140.83, 131.55, 124.71, 124.49. Elem. Anal. Calcd. for $C_8H_4ClN_3O_2$: C, 45.85; H, 1.92; N 20.05. Found: C, 45.54; H, 1.89; N 19.86.

(c) To a solution of 2-chloro-7-nitroquinoxaline (**3**) (4.43 g, 21.1 mmol) in EtOAc (70 mL) was added $SnCl_2.2H_2O$ (16.7 g, 74 mmol) and the reaction mixture was refluxed for 2 h. After cooling to room temperature, 50% aqueous solution of NaOH (50 mL) was added to the reaction mixture dropwise at 0 °C and the reaction mixture was poured on a pad of silica gel, then eluted with hot acetone (100 mL). The filtrate was concentrated, and product was purified by column chromatography (mobile phase: hexane/EtOAc, 2.5:1) to give 3-chloroquinoxalin-6-amine (**4**) as a yellow solid in 57% yield; mp 206-208 °C (lit mp (Lassagne et al. 2020) 210-212 °C). ^{1}H NMR (600 MHz, DMSO) δ 8.38 (s, 1H), 7.72 (d, J = 9.0 Hz, 1H), 7.21 (dd, J = 2.5, 9.0 Hz, 1H), 6.77 (d, J = 2.4 Hz, 1H), 6.30 (s,

2H). ^{13}C NMR (151 MHz, DMSO) δ 152.55, 147.08, 144.84, 138.45, 135.25, 130.20, 123.01, 104.33. Elem. Anal. Calcd. for $C_8H_6ClN_3$: C, 53.50; H, 3.37; N 23.40. Found: C, 53.43; H, 3.34; N 23.20.

Synthesis of *N*-(3-chloroquinoxalin-6-yl)acetamide (5)

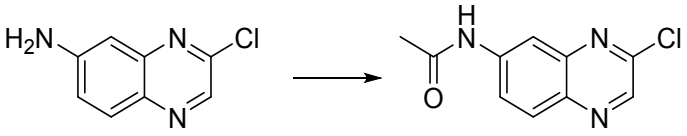

4 **5**

A solution of acetyl chloride (0.21 g/0.19 mL, 2.6 mmol) in $CHCl_3$ (5 mL) was added dropwise to a solution of 3-chloroquinoxalin-6-amine (**4**) (0.24 g, 1.3 mmol) and sodium carbonate (0.43 g, 3.9 mmol) in $CHCl_3$ (20 mL). The mixture was refluxed for 4 h. After cooling, reaction mixture was filtered off, the filtrate was concentrated under reduced pressure. The product was washed with diethyl ether (15 mL) and dried over P_2O_5. *N*-(3-Chloroquinoxalin-6-yl)acetamide (**5**) was obtained in 80% yield as a light beige solid; mp 204-205 °C. ^{1}H NMR (600 MHz, DMSO) 10.50 (s, 1H), 8.78 (s, 1H), 8.36 (d, *J* = 2.3 Hz, 1H), 8.02 (d, *J* = 9.0 Hz, 1H), 7.88 (dd, *J* = 2.3, 9.1 Hz, 1H), 2.11 (s, 3H). ^{13}C NMR (151 MHz, DMSO) δ 169.87, 147.72, 143.62, 142.83, 142.29, 137.77, 129.98, 124.33, 114.54, 24.78. Elem. Anal. Calcd. for $C_{10}H_8ClN_3O$: C, 54.19; H, 3.64; N 18.96. Found: C, 54.40; H, 3.48; N 18.78.

Synthesis of 2-chloro-7-iodoquinoxaline (6)

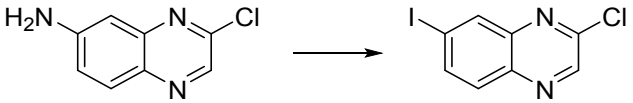

4 **6**

3-Chloroquinoxalin-6-amine (**4**) (0.5 g, 2.8 mmol) was added to a solution of *p*-toluenesulfonic acid monohydrate (1.6 g, 8.4 mmol) in acetonitrile (20 mL) and the reaction mixture was cooled to 10 °C. The solution of sodium nitrite (0.39 g, 5.6 mmol) and potassium iodide (1.16 g, 7.0 mmol) in water (10 mL) was added dropwise. The reaction mixture was stirred at 10 °C for 10 min, and then 2 h at room temperature. The reaction mixture was diluted with water (70 mL) and 1M $NaHCO_3$ was dropped to achieve pH = 10, then 2M $Na_2S_2O_3$ (6 mL) was added. The reaction mixture was extracted with EtOAc (3 × 50 mL). The organic layer was then washed with water (1 × 30 mL) and brine (1 × 30 mL), dried over anhydrous sodium sulfate and concentrated. The product was purified by column chromatography (mobile phase: hexane/$CHCl_3$, 1:1) to give 2-chloro-7-iodoquinoxaline (**6**) in 54% yield as a white solid; mp 146-147 °C (lit mp (Hazeldine et al. 2001) 148-150 °C). ^{1}H NMR (500 MHz, DMSO) δ 9.01 (s, 1H), 8.47 (d, *J* = 1.9 Hz, 1H), 8.16 (dd, *J* = 1.9, 8.7 Hz, 1H), 7.90 (d, *J* = 8.7 Hz, 1H). ^{13}C NMR (126 MHz, DMSO) δ 147.62, 146.15, 142.09, 139.86, 139.38, 136.69, 130.61, 98.96. Elem. Anal. Calcd. for $C_8H_4ClIN_2$: C, 33.08; H, 1.39; N 9.64. Found: C, 33.34; H, 1.58; N 9.37.

Synthesis of XK469 analogues

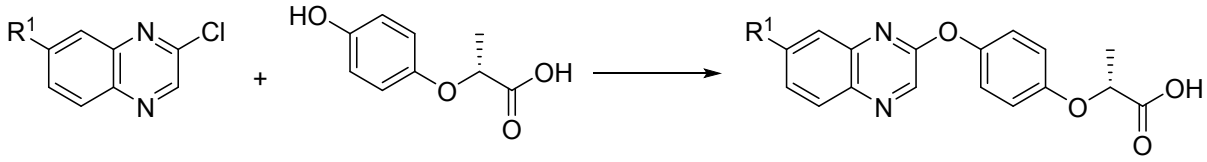

R^1 = -H: **JM-73**
R^1 = -Br: **JM-228**
R^1 = -CH_3: **JM-229**
R^1 = -CH_3O: **JM-230**
R^1 = -I: **JM-178**
R^1 = -$NHCOCH_3$: **JM-108**

(*R*)-2-(4-(Quinoxalin-2-yloxy)phenoxy)propanoic acid (JM-73)

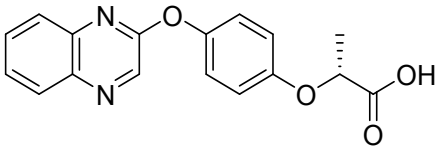

The mixture of (*R*)-2-(4-hydroxyphenoxy)propanoic acid (0.14 g, 0.75 mmol) and potassium carbonate (0.21 g, 1.5 mmol) was stirred in DMF (7 mL) at 75 °C for 2 h. Then, 2-chloroquinoxaline (0.08 g, 0.5 mmol) was added and reaction mixture was heated to 145 °C for 2 h. After reaction completion, the reaction mixture was poured into ice water (50 mL), acidified to pH 3-4 and extracted with EtOAc (3 × 30 mL). The organic layer was additionally washed with water (2 × 20 mL) and brine (1 × 20 mL), dried over anhydrous sodium sulfate and concentrated. The product was suspended with diethyl ether and filtered off. (*R*)-2-(4-(Quinoxalin-2-yloxy)phenoxy)propanoic acid was obtained in 67% yield as a white solid; mp 162-163 °C. ^{1}H NMR (500 MHz, DMSO) δ 13.07 (s, 1H), 8.83 (s, 1H), 8.05 (d, *J* = 7.8 Hz, 1H), 7.72 (d, *J* = 3.7 Hz, 2H), 7.70-7.66 (m, 1H), 7.26-7.23 (m, 2H), 6.98-6.95 (m, 2H), 4.86 (q, *J* = 6.7 Hz, 1H), 1.53 (d, *J* = 6.8 Hz, 3H). ^{13}C NMR (126 MHz, DMSO) δ 173.29, 157.29, 155.07, 146.21, 139.91, 139.44, 139.18, 130.82, 128.83, 127.71, 127.35, 122.79, 115.81, 72.01, 18.52. Elem. Anal. Calcd. for $C_{17}H_{14}N_2O_4$: C, 65.80; H, 4.55; N, 9.03. Found: C, 65.52; H, 4.69; N, 8.86.

(*R*)-2-(4-((7-Bromoquinoxalin-2-yl)oxy)phenoxy)propanoic acid (JM-228)

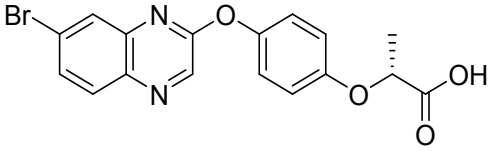

The mixture of (*R*)-2-(4-hydroxyphenoxy)propanoic acid (0.14 g, 0.75 mmol) and potassium carbonate (0.21 g, 1.5 mmol) was stirred in DMF (7 mL) at 75 °C for 2 h. Then, 7-bromo-2-chloroquinoxaline (0.12 g, 0.5 mmol) was added and reaction mixture was heated to 145 °C for 6 h. After reaction completion, the reaction mixture was poured into ice water (50 mL), acidified to pH 3-4 and extracted with EtOAc (3 × 30 mL). The organic layer was additionally washed with water (2 × 20 mL) and brine (1 × 20 mL), dried over anhydrous sodium sulfate and concentrated. The product was purified by column chromatography (mobile phase: hexane/EtOAc, 1:1). (*R*)-2-(4-((7-Bromoquinoxalin-2-yl)oxy)phenoxy)propanoic acid was obtained in 48 % yield as a white solid; mp 194-196 °C. ^{1}H NMR (500 MHz, DMSO) δ 8.85 (s, 1H), 7.98 (d, *J* = 8.8 Hz, 1H), 7.94 (d, *J* = 2.2 Hz, 1H), 7.81 (dd,

J = 2.2, 8.8 Hz, 1H), 7.26-7.23 (m, 2H), 6.97-6.94 (m, 2H), 4.84 (q, J = 6.7 Hz, 1H), 1.52 (d, J = 6.7 Hz, 3H). ^{13}C NMR (126 MHz, DMSO) δ 173.61, 158.05, 155.50, 146.26, 140.95, 140.71, 138.30, 131.13, 130.90, 129.69, 124.15, 122.98, 116.10, 72.40, 18.83. Elem. Anal. Calcd. for $C_{17}H_{13}BrN_2O_4$: C, 52.46; H, 3.37; N, 7.20. Found: C, 52.18; H, 3.18; N, 7.04.

(*R*)-2-(4-((7-Methylquinoxalin-2-yl)oxy)phenoxy)propanoic acid (JM-229)

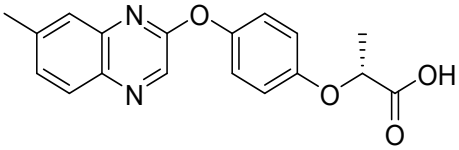

The mixture of (*R*)-2-(4-hydroxyphenoxy)propanoic acid (0.14 g, 0.75 mmol) and potassium carbonate (0.21 g, 1.5 mmol) was stirred in DMF (7 mL) at 75 °C for 2 h. Then, 2-chloro-7-methylquinoxaline (0.09 g, 0.5 mmol) was added and reaction mixture was heated to 145 °C for 6 h. After reaction completion, the reaction mixture was poured into ice water (50 mL), acidified to pH 3-4 and extracted with EtOAc (3 × 30 mL). The organic layer was additionally washed with water (2 × 20 mL) and brine (1 × 20 mL), dried over anhydrous sodium sulfate and concentrated. The product was purified by column chromatography (mobile phase: hexane/EtOAc, 1:1). (*R*)-2-(4-((7-Methylquinoxalin-2-yl)oxy)phenoxy)propanoic acid was obtained in 40% yield as a white solid; mp 190-192 °C (lit mp (Hazeldine et al. 2001) 178-180 °C). ^{1}H NMR (500 MHz, DMSO) δ 8.73 (s, 1H), 7.93 (d, J = 8.3 Hz, 1H), 7.54-7.49 (m, 2H), 7.24-7.21 (m, 2H), 6.97-6.93 (m, 2H), 4.85 (q, J = 6.7 Hz, 1H), 2.46 (s, 3H), 1.53 (d, J = 6.8 Hz, 3H). ^{13}C NMR (126 MHz, DMSO) δ 173.38, 157.43, 155.06, 146.24, 141.14, 139.50, 138.67, 137.60, 129.64, 128.38, 126.51, 122.80, 115.76, 72.07, 21.30, 18.57. Elem. Anal. Calcd. for $C_{18}H_{16}N_2O_4$: C, 66.66; H, 4.97; N, 8.64. Found: C, 66.47; H, 4.81, N 8.36.

(*R*)-2-(4-((7-Methoxyquinoxalin-2-yl)oxy)phenoxy)propanoic acid (JM-230)

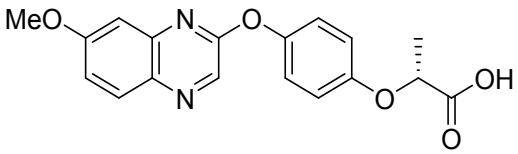

The mixture of (*R*)-2-(4-hydroxyphenoxy)propanoic acid (0.14 g, 0.75 mmol) and potassium carbonate (0.21 g, 1.5 mmol) was stirred in DMF (7 mL) at 75 °C for 2 h. Then, 2-chloro-7-methoxyquinoxaline (0.10 g, 0.5 mmol) was added and reaction mixture was heated to 145 °C for 6 h. After reaction completion, the reaction mixture was poured into ice water (50 mL), acidified to pH 3-4 and extracted with EtOAc (3 × 30 mL). The organic layer was additionally washed with water (2 × 20 mL) and brine (1 × 20 mL), dried over anhydrous sodium sulfate and concentrated. The product was purified by column chromatography (mobile phase: hexane/EtOAc, 1:3). (*R*)-2-(4-((7-Methoxyquinoxalin-2-yl)oxy)phenoxy)propanoic acid was obtained in 62% yield as a white solid; mp 138-140 °C. ^{1}H NMR (600 MHz, DMSO) δ 13.02 (s, 1H), 8.59 (s, 1H), 7.89 (d, J = 9.1 Hz, 1H), 7.25 (dd, J = 2.8, 9.1 Hz, 1H), 7.20-7.18 (m, 2H), 7.06 (d, J = 2.8 Hz, 1H), 6.93-6.91 (m, 2H), 4.82 (q, J = 6.8 Hz, 1H), 3.82 (s, 3H), 1.50 (d, J = 6.8 Hz, 3H). ^{13}C NMR (151 MHz, DMSO) δ 173.68, 161.50, 158.15, 155.42, 146.67, 141.79, 136.71, 135.25, 130.17, 123.21, 120.07, 116.16, 106.68, 72.37, 56.42, 18.90. Elem. Anal. Calcd. for $C_{18}H_{16}N_2O_5$: C, 63.53; H, 4.74; N, 8.23. Found: C, 63.35; H, 4.63, N 7.95.

(*R*)-2-(4-((7-Iodoquinoxalin-2-yl)oxy)phenoxy)propanoic acid (JM-178)

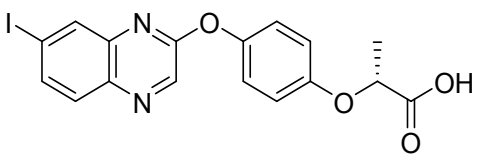

The mixture of (*R*)-2-(4-hydroxyphenoxy)propanoic acid (0.14 g, 0.75 mmol) and potassium carbonate (0.21 g, 1.5 mmol) was stirred in DMF (7 mL) at room temperature for 30 min and then was heated to 75 °C for 2 h. Then, 2-chloro-7-iodoquinoxaline (**6**) (0.14 g, 0.5 mmol) was added and reaction mixture was heated to 145 °C for 6 h. After reaction completion, the reaction mixture was poured into ice water (50 mL), acidified to pH 3-4 and extracted with EtOAc (3 × 30 mL). The organic layer was additionally washed with water (2 × 20 mL) and brine (1 × 20 mL), dried over anhydrous sodium sulfate and concentrated. The product was purified by column chromatography (mobile phase: hexane/EtOAc/CH_3COOH, 10:10:1). (*R*)-2-(4-((7-Iodoquinoxalin-2-yl)oxy)phenoxy)propanoic acid was obtained in 57% yield as a light beige solid; mp 170-172 °C (lit mp (Hazeldine et al. 2001) 164-166 °C). ^{1}H NMR (500 MHz, DMSO) δ 8.81 (s, 1H), 8.10 (d, *J* = 1.9 Hz, 1H), 7.92 (dd, *J* = 1.9, 8.7 Hz, 1H), 7.78 (d, *J* = 8.7 Hz, 1H), 7.21-7.17 (m, 2H), 6.93-6.90 (m, 2H), 4.67 (q, *J* = 6.7 Hz, 1H), 1.47 (d, *J* = 6.8 Hz, 3H). ^{13}C NMR (126 MHz, DMSO) δ 173.84, 157.52, 155.70, 145.55, 140.61, 140.48, 138.30, 136.22, 135.69, 130.33, 122.46, 115.67, 97.53, 73.25, 18.82. Elem. Anal. Calcd. for $C_{17}H_{13}IN_2O_4$: C, 46.81; H, 3.00; N, 6.42. Found: C, 46.48; H, 2.81; N, 6.63.

(*R*)-2-(4-((7-Acetamidoquinoxalin-2-yl)oxy)phenoxy)propanoic acid (JM-108)

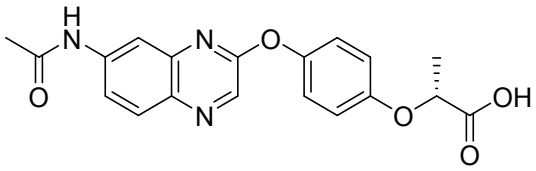

The mixture of (*R*)-2-(4-hydroxyphenoxy)propanoic acid (0.14 g, 0.75 mmol) and potassium carbonate (0.21 g, 1.5 mmol) was stirred in DMF (7 mL) at room temperature for 30 min and then was heated to 75 °C for 2 h. Then, *N*-(3-chloroquinoxalin-6-yl)acetamide (**5**) (0.11 g, 0.5 mmol) was added and reaction mixture was heated to 145 °C for 6 h. After reaction completion, the reaction mixture was poured into ice water (50 mL), acidified to pH 3-4 and extracted with EtOAc (3 × 30 mL). The organic layer was additionally washed with water (2 × 20 mL) and brine (1 × 20 mL), dried over anhydrous sodium sulfate and concentrated. The product was purified by column chromatography (mobile phase: hexane/EtOAc/CH_3COOH, 5:5:1). (*R*)-2-(4-((7-Acetamidoquinoxalin-2-yl)oxy)phenoxy)propanoic acid was obtained in 67% yield as a light beige solid; mp 243-244 °C. ^{1}H NMR (600 MHz, DMSO) δ 10.50 (s, 1H), 8.57 (s, 1H), 8.08 (d, *J* = 2.3 Hz, 1H), 7.89 (d, *J* = 8.9 Hz, 1H), 7.65 (dd, *J* = 2.3, 9.1 Hz, 1H), 7.09-7.08 (m, 2H), 6.86-6.85 (m, 2H), 4.39 (q, *J* = 6.9 Hz, 1H), 2.05 (s, 3H), 1.40 (d, *J* = 6.7 Hz, 3H). ^{13}C NMR (151 MHz, DMSO) δ 175.35, 169.61, 158.18, 156.62, 145.58, 141.63, 140.77, 137.73, 136.04, 129.39, 122.63, 120.92, 115.97, 114.39, 75.41, 24.70, 19.60. Elem. Anal. Calcd. for $C_{19}H_{17}N_3O_5$: C, 62.12; H, 4.66; N, 11.44. Found: C, 61.89; H, 4.32; N, 11.51.

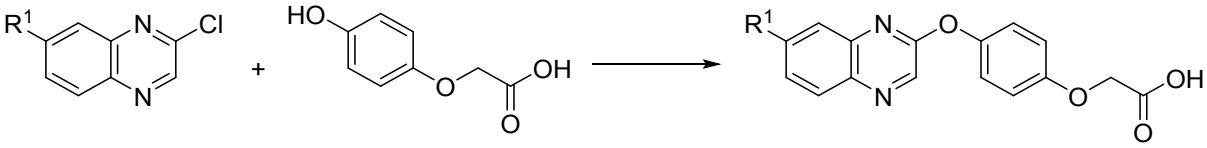

R^1 = H: **JM-85**
R^1 = -I: **JM-177**
R^1 = -NHCOCH$_3$: **JM-107**

2-(4-(Quinoxalin-2-yloxy)phenoxy)acetic acid (JM-85)

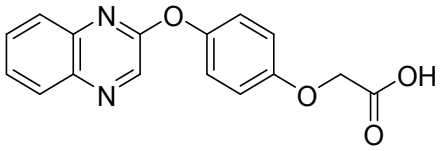

The mixture of 2-(4-hydroxyphenoxy)acetic acid (0.13 g, 0.75 mmol) and potassium carbonate (0.21 g, 1.5 mmol) was stirred in DMF (7 mL) at room temperature for 30 min and then was heated to 75 °C for 2 h. Then, 2-chloroquinoxaline (0.08 g, 0.5 mmol) was added and reaction mixture was heated to 145 °C for 2 h. After reaction completion, the reaction mixture was poured into ice water (50 mL), acidified to pH 3-4 and extracted with EtOAc (3 × 30 mL). The organic layer was additionally washed with water (2 × 20 mL) and brine (1 × 20 mL), dried over anhydrous sodium sulfate and concentrated. The product was suspended with diethyl ether and filtered off. 2-(4-(Quinoxalin-2-yloxy)phenoxy)acetic acid was obtained in 64% yield as a white solid; mp 185-187 °C. ^{1}H NMR (500 MHz, DMSO) δ 8.81 (s, 1H), 8.05 (d, *J* = 7.6 Hz, 1H), 7.74-7.66 (m, 3H), 7.26-7.22 (m, 2H), 7.02-6.99 (m, 2H), 4.71 (s, 2H). ^{13}C NMR (126 MHz, DMSO) δ 170.56, 157.44, 155.47, 146.40, 140.01, 139.55, 139.27, 131.00, 128.94, 127.88, 127.45, 122.91, 115.66, 65.10. Elem. Anal. Calcd. for $C_{16}H_{12}N_2O_4$: C, 64.86; H, 4.08; N, 9.46. Found: C, 64.78; H, 3.91; N, 9.50.

2-(4-((7-Iodoquinoxalin-2-yl)oxy)phenoxy)acetic acid (JM-177)

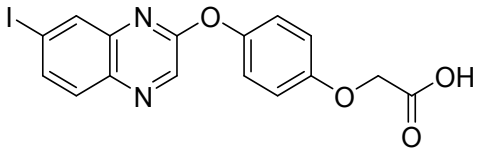

The mixture of 2-(4-hydroxyphenoxy)acetic acid (0.13 g, 0.75 mmol) and potassium carbonate (0.21 g, 1.5 mmol) was stirred in DMF (7 mL) at room temparature for 30 min and then was heated to 75 °C for 2 h. Then, 2-chloro-7-iodoquinoxaline (**6**) (0.14 g, 0.5 mmol) was added and reaction mixture was heated to 145 °C for 6 h. After reaction completion, the reaction mixture was poured into ice water (50 mL), acidified to pH 3-4 and extracted with EtOAc (3 × 30 mL). The organic layer was additionally washed with water (2 × 20 mL) and brine (1 × 20 mL), dried over anhydrous sodium sulfate and concentrated. The product was purified by column chromatography (mobile phase: hexane/EtOAc/CH_3COOH, 10:10:1). 2-(4-((7-Iodoquinoxalin-2-yl)oxy)phenoxy)acetic acid was obtained in 62% yield as a white solid; mp 177-178 °C. ^{1}H NMR (500 MHz, DMSO) δ 8.83 (s, 1H), 8.10 (d, *J* = 1.8 Hz, 1H), 7.94 (dd, *J* = 1.9, 8.6 Hz, 1H), 7.80 (d, *J* = 8.7 Hz, 1H), 7.26-7.23 (m, 2H), 7.01-6.98 (m, 2H), 4.69 (s, 2H). ^{13}C NMR (126 MHz, DMSO) δ 170.45, 157.51, 155.53, 146.05, 140.65, 140.48, 138.36, 136.30, 135.69, 130.38, 122.66, 115.53, 97.59, 65.19. Elem. Anal. Calcd. for $C_{16}H_{11}IN_2O_4$: C, 45.52; H, 2.63; N, 6.64. Found: C, 45.37; H, 2.49; N, 6.50.

2-(4-((7-Acetamidoquinoxalin-2-yl)oxy)phenoxy)acetic acid (JM-107)

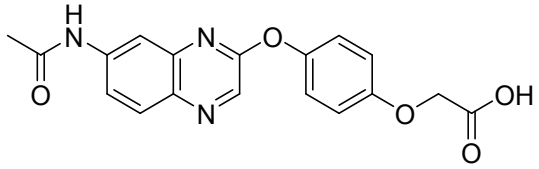

The mixture of 2-(4-hydroxyphenoxy)acetic acid (0.13 g, 0.75 mmol) and potassium carbonate (0.21 g, 1.5 mmol) was stirred in DMF (7 mL) at room temperature for 30 min and then was heated to 75 °C for 2 h. Then, *N*-(3-chloroquinoxalin-6-yl)acetamide (**5**) (0.11 g, 0.5 mmol) was added and reaction mixture was heated to 145 °C for 6 h. After reaction completion, the reaction mixture was poured into ice water (50 mL), acidified to pH 3-4 and extracted with EtOAc (3 × 30 mL). The organic layer was additionally washed with water (2 × 20 mL) and brine (1 × 20 mL), dried over anhydrous sodium sulfate and concentrated. The product was purified by column chromatography (mobile phase: hexane/EtOAc/CH_3COOH, 5:5:1). 2-(4-((7-Acetamidoquinoxalin-2-yl)oxy)phenoxy)acetic acid was obtained in 67% yield as a light pink solid; mp 216-218 °C. ^{1}H NMR (500 MHz, DMSO) δ 10.39 (s, 1H), 8.66 (s, 1H), 8.14 (d, J = 2.3 Hz, 1H), 7.96 (d, J = 9.0 Hz, 1H), 7.67 (dd, J = 2.2, 9.0 Hz, 1H), 7.25-7.22 (m, 2H), 7.02-6.99 (m, 2H), 4.72 (s, 2H), 2.10 (s, 3H). ^{13}C NMR (126 MHz, DMSO) δ 170.42, 169.30, 162.55, 157.77, 155.33, 146.29, 141.22, 140.40, 137.52, 135.80, 129.18, 122.81, 120.61, 115.56, 114.06, 65.06, 24.42. Elem. Anal. Calcd. For $C_{18}H_{15}N_3O_5$: C, 61.19; H, 4.28; N, 11.89. Found: C, 61.35; H, 4.33; N, 11.76.

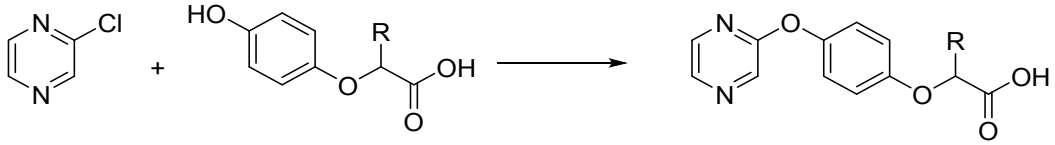

R = H: **JM-109**
R = (*R*)-CH_3: **JM-110**

2-(4-(Pyrazin-2-yloxy)phenoxy)acetic acid (JM-109)

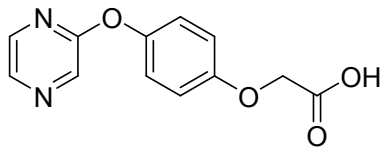

The mixture of 2-(4-hydroxyphenoxy)acetic acid (0.13 g, 0.75 mmol) and potassium carbonate (0.21 g, 1.5 mmol) was stirred in DMF (7 mL) at room temperature for 30 min and then was heated to 75 °C for 2 h. Then, 2-chloropyrazine (0.06 g, 0.5 mmol) was added and reaction mixture was heated to 145 °C for 6 h. After reaction completion, the reaction mixture was poured into ice water (50 mL), acidified to pH 3-4 and extracted with EtOAc (3 × 30 mL). The organic layer was additionally washed with water (2 × 20 mL) and brine (1 × 20 mL), dried over anhydrous sodium sulfate and concentrated. The product was purified by column chromatography (mobile phase: hexane/EtOAc/CH_3COOH, 10:10:1). 2-(4-(Pyrazin-2-yloxy)phenoxy)acetic acid was obtained in 78% yield as a light beige solid; mp 194-196 °C. ^{1}H NMR (500 MHz, DMSO) δ 8.49 (d, J = 1.4 Hz, 1H), 8.33 (d, J = 2.7 Hz, 1H), 8.17 (dd, J = 1.4, 2.7 Hz, 1H), 7.13-7.09 (m, 2H), 6.95-6.92 (m, 2H), 4.59 (s, 2H). ^{13}C NMR (126 MHz, DMSO) δ 170.64, 160.21, 155.51, 146.39, 141.31, 138.73, 135.51, 122.53, 115.54, 65.65. Elem. Anal. Calcd. for $C_{12}H_{10}N_2O_4$: C, 58.54; H, 4.09; N, 11.38. Found: C, 58.19; H, 4.23; N, 11.20.

(*R*)-2-(4-(Pyrazin-2-yloxy)phenoxy)propanoic acid (JM-110)

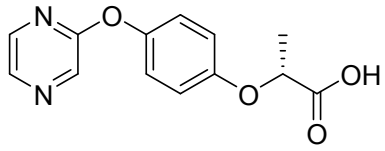

The mixture of (*R*)-2-(4-hydroxyphenoxy)propanoic acid (0.14 g, 0.75 mmol) and potassium carbonate (0.21 g, 1.5 mmol) was stirred in DMF (7 mL) at room temperature for 30 min and then was heated to 75 °C for 2 h. 2-Chloropyrazine (0.06 g, 0.5 mmol) was added and reaction mixture was heated to 145 °C for 6 h. After reaction completion, the reaction mixture was poured into ice water (50 mL), acidified to pH 3-4 and extracted with EtOAc (3 × 30 mL). The organic layer was additionally washed with water (2 × 20 mL) and brine (1 × 20 mL), dried over anhydrous sodium sulfate and concentrated. The product was purified by column chromatography (mobile phase: hexane/EtOAc/CH_3COOH, 10:10:1). (*R*)-2-(4-(Pyrazin-2-yloxy)phenoxy)propanoic acid was obtained in 76% yield as a light beige solid; mp 131-133 °C. ^{1}H NMR (500 MHz, DMSO) δ 13.03 (s, 1H), 8.49 (d, *J* = 1.4 Hz, 1H), 8.33 (d, *J* = 2.8 Hz, 1H), 8.17 (dd, *J* = 1.4, 2.8 Hz, 1H), 7.13-7.10 (m, 2H),6.93-6.90 (m, 2H), 4.81 (q, *J* = 6.7 Hz, 1H), 1.50 (d, *J* = 6.8 Hz, 3H). ^{13}C NMR (126 MHz, DMSO) δ 173.29, 160.14, 154.96, 146.50, 141.28, 138.75, 135.52, 122.59, 115.88, 72.16, 18.50. Elem. Anal. Calcd. for $C_{13}H_{12}N_2O_4$: C, 60.00; H, 4.65; N, 10.76. Found: C, 59.82; H, 4.53; N, 10.59.

1.2 CRISPR-Cas9 mediated deletion of TOP2B in HL-60

CRISPR-Cas9 mediated deletion of TOP2B in HL-60 was performed according to Khazeem et al. (2022; 2020). Shortly, HL-60 cells were transfected with the plasmid encoding Cas9 protein, selected gRNA targeting the sequence of the first exon of TOP2B gene and green fluorescent protein (GFP) sequence to enable fluorescence-activated cell sorting (FACS). After that, single-cell colonies were genotyped to search for the mutation causing the TOP2B depletion. TOP2B protein depletion was also confirmed using western blotting and immunofluorescence.

1.3 LC-MS assay of XK469 in rabbit plasma

A pilot pharmacokinetic experiment was performed with two rabbits for a dosing setup of compound XK469 in rabbits *in vivo*. Compound XK469 (in the form of sodium salt containing 5 mg/kg XK469 free acid) was dissolved in saline and after filtration (0.22 nm) administered intravenously to the marginal ear vein of rabbits. Rabbit plasma (50 µL) was spiked with an internal standard (diclofenac), precipitated with ice-cold methanol (250 µL), vortexed (30 s), and centrifuged (10 min, 10,000 rpm, 4 °C). The resulting supernatant was filtered through a 0.45 µm porosity filter (Milex – Hv, Merck-Milipore, Darmstadt, Germany) and analyzed. NexeraX2 UHPLC with an LCMS-8030 triple quadrupole mass spectrometer (Shimadzu, Kyoto, Japan) working in a positive ionization mode was used. Separation was achieved on an Acquity UPLC BEH C18 (50 × 2.1 mm, 1.7 µm, Waters, Dublin, Ireland) with the mobile phase composed of 0.5% formic acid (part A) and acetonitrile (part B) in the following gradient: 0-3 min (35-80% B), 3-4 (95% B), 4-4.1 min (95-35% B), 4.1-5.5 min (35% B). Quantification was performed in the selected reaction monitoring (see table below). Linearity was verified within the concentration range of 3 to 300 µM of XK469 in rabbit plasma, and linear fits using weighted standard curves (1/x) with corresponding $R^2 > 0.99$ were obtained. Maximal plasma concentration (c_{max}) of XK469 (159 and 177 µM) was found 5 min after

drug administration with a relatively slow decline in the elimination phase (8 h post-dose the plasma concentrations were 38 and 42 % of their c_{max}, respectively) (Figure S4). Based on this data the dose of XK469 for pharmacodynamic investigations was only slightly increased to 6 mg/kg for further *in vivo* experiments.

Analyte	**Precursor ion** (m/z)	**Product ions** (m/z)	**Collision energy** (eV)
XK469	344.85	298.95, 163.8, 136.9	20, 41, 55
I.S.	296.2	249.85, 214.9	14, 21

I.S. – internal standard

1.4 Echocardiographic parameters and their determinations

Following formulas (1-6) were used for determination of echocardiographic parameters presented in the present study (Table 1), where LVEF is left ventricular ejection fraction, LVIDd and LVIDs are left ventricular internal diameters at end diastole and end systole, LVV is left ventricular volume at end diastole and end systole (LVVd and LVVs), LVEF is left ventricular ejection fraction, CO is cardiac output, SV is stroke volume, HR is heart rate, LVM is left ventricular mass, IVSd is interventricular septum thickness at end diastole and LVPW – left ventricular posterior wall thickness at end diastole.

$$(1)\ LVFS\ (\%) = \frac{LVIDd - LVIDs}{LVIDd} \times 100$$

$$(2)\ LVV = \left(\frac{7.0}{(2.4 + LVID)}\right) \times LVID^3$$

$$(3)\ LVEF\ (\%) = \frac{LVVd - LVVs}{LVVd} \times 100$$

$$(4)\ SV = LVDd - LVDs$$

$$(5)\ CO = SV \times HR$$

$$(6)\ LVM = 0.8 \times 1.04 \times \left[(IVSd + LVIDd + LVPWd)^3\, LVIDd^3\right] + 0.6$$

2 SUPPLEMENTAL FIGURES

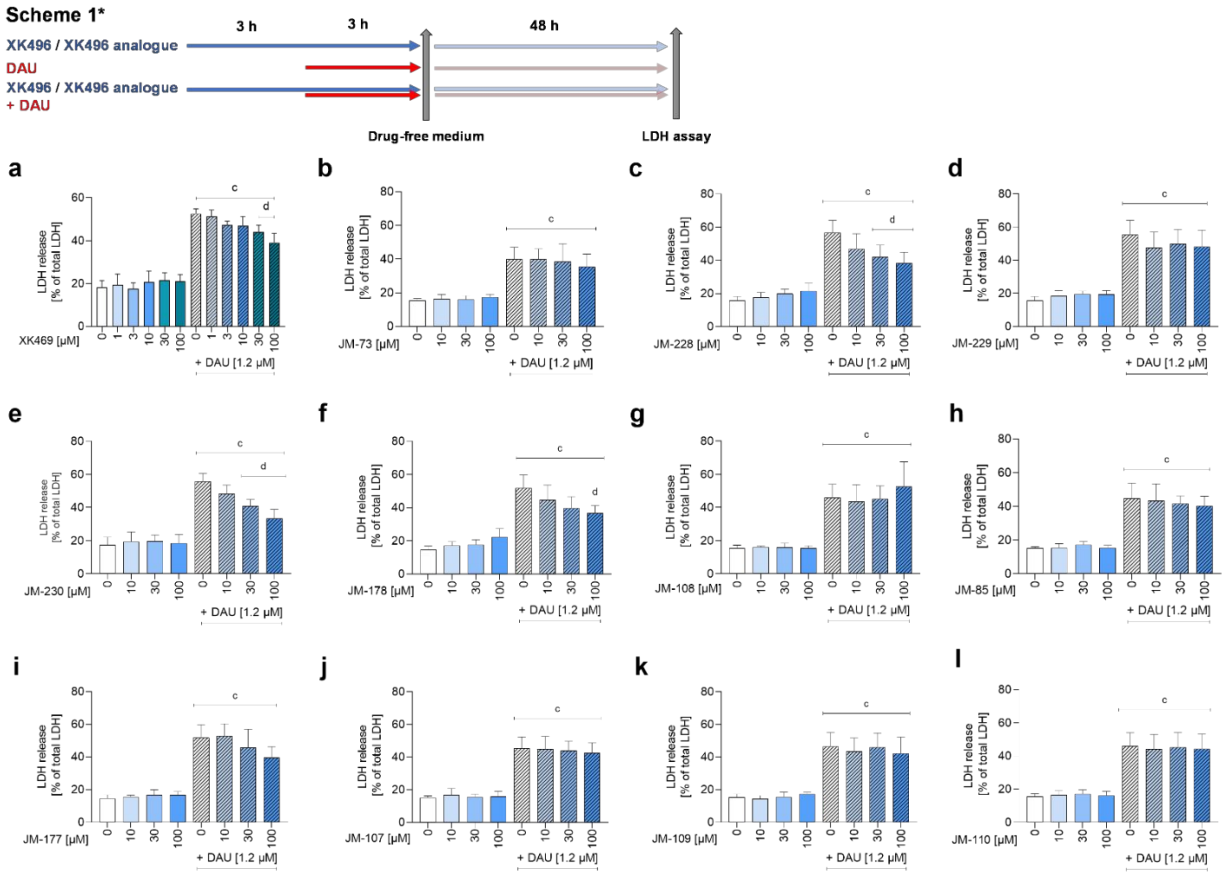

Fig. S1 *Cytotoxicity/protection of XK469 analogues on primary cardiomyocytes.* cardiomyocytes were incubated with XK469 analogues (10; 30; 100 µM), 1.2 µM daunorubicin or their combination in well-established scheme that was modified from Hasinoff (2002). Drug toxicity was evaluated as percentage of lactate dehydrogenase leaked to the culture media which corresponds to the percentage of damaged cells. Statistical analyses: n = 4, mean ± SD, statistical significance: ”c” - compared to drug-free control, ”d” - compared to daunorubicin, One-way Anova, Holm-Sidak´s post-test, $P \leq 0.05$

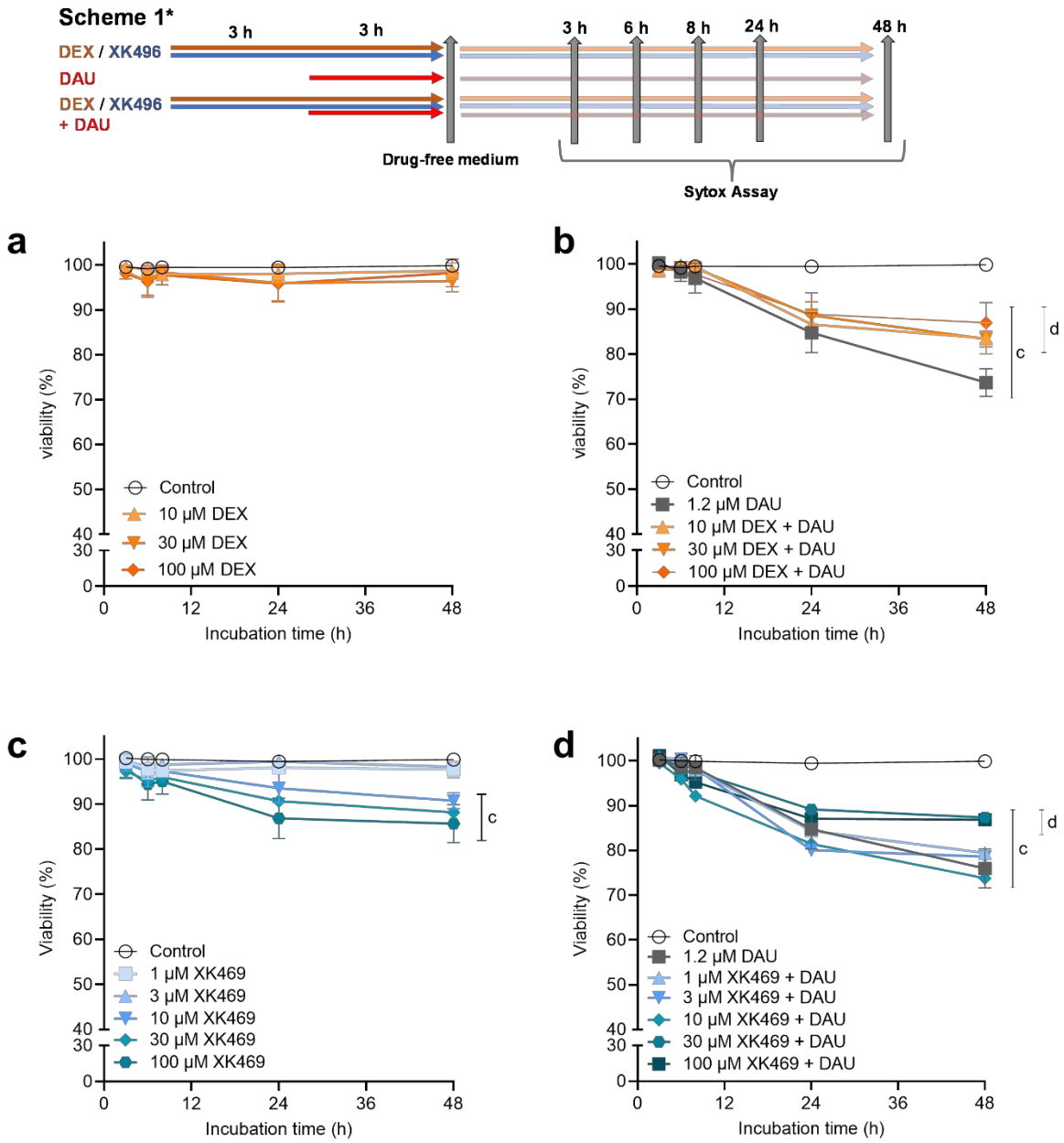

Fig. S2 *Scheme 1* Cytotoxicity/protection of dexrazoxane (DEX) and XK469 on primary cardiomyocytes.* Cardiomyocytes were incubated with DEX (*a, b*) and XK469 (*c, d*) for 3 h and then co-incubated with daunorubicin (DAU) for next 3 h, followed by 48 h in drug-free media. Drug toxicity was evaluated using Sytox Green Cytotoxicity Assay. Statistical analysis: $n \geq 4$, mean ± SD, One-way ANOVA, Dunn's post hoc test, $P \leq 0.05$; "c" – compared to control; "d" – compared to DAU

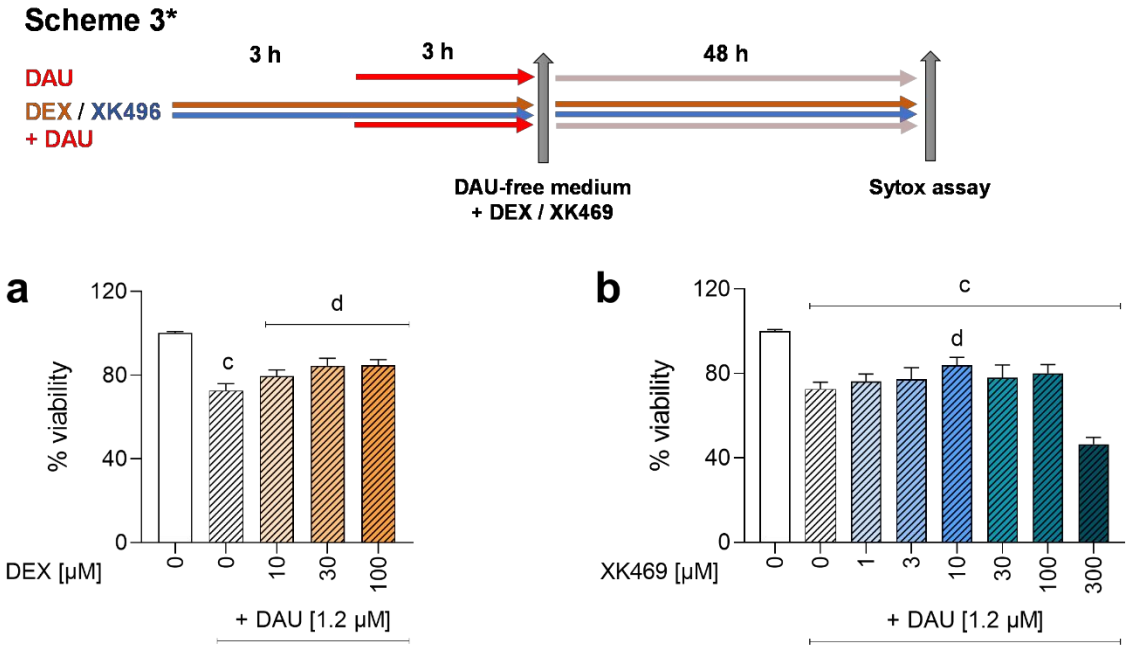

Fig. S3 *Scheme 3* Cytoxicity/protection of XK469 and dexrazoxane (DEX) on primary cardiomyocytes.* Cardiomyocytes were incubated with various concentrations of DEX (*a*) and XK469 (*b*) for 3 h and then co-incubated with daunorubicin (DAU) for 3 h, following by 48h incubation with DEX or XK469 alone. Statistical analysis: n ≥ 4, mean ± SD, One-way ANOVA, Dunn's post hoc test, P ≤ 0.05; "c" – compared to control; "d" – compared to DAU

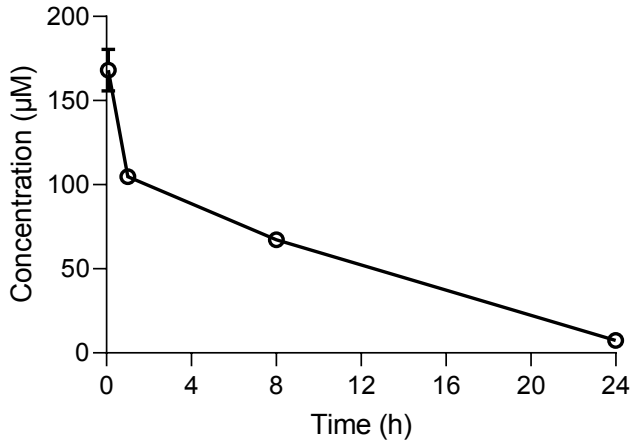

Fig. S4 *Pilot pharmacokinetic study of XK469 in vivo.* Rabbits were treated with 5 mg/kg XK469 (*i.v.*) Plasma concentrations of XK469 after 5 min, 1 h, 8 h, and 24 h post administration were determined using LC-MS. The experiment was performed in biological duplicates.

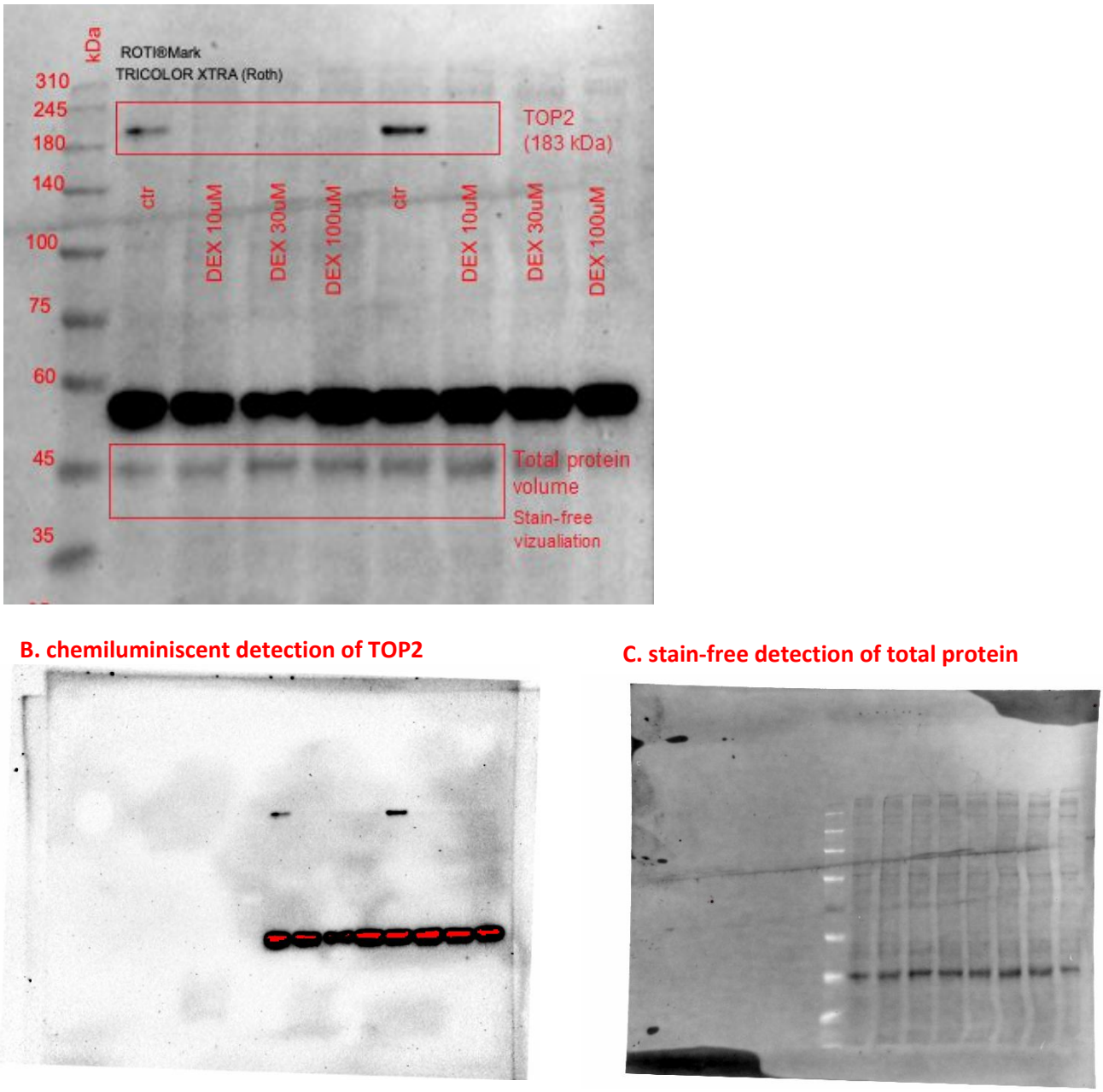

Fig. S5 *Representative membrane of the TOP2 immunodetection.* Merged signal of chemiluminescence, fluorescent and colorimetric detection (A), chemiluminescent detection of TOP2 (B), stain-free detection of total protein (C). Antibodies: rabbit anti-TOP2A/B (1: 2,000, ab109524, Abcam, U.K.) and HRP-labelled F(ab')2 goat anti-rabbit IgG (1:10,000, ab6112, Abcam, U.K.); normalization to the total protein volume (Bio-Rad, U.S.A.)

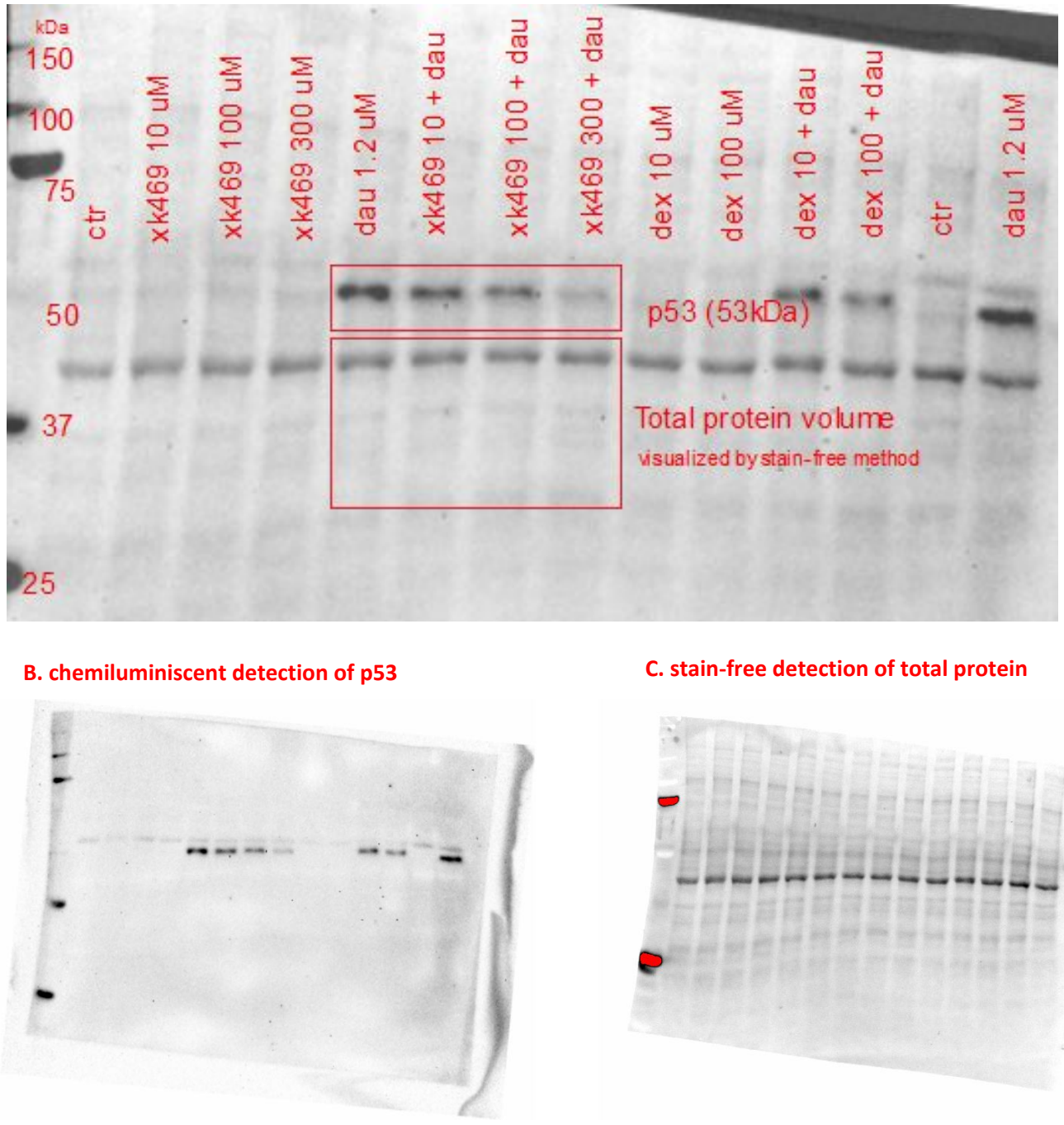

Fig. S6 *Representative membrane of the phospho-p53 [pSer392] immunodetection in vitro.* Merged signal of chemiluminescence, fluorescent and colorimetric detection(A), chemiluminescent detection of phospho-p53 (B), stain-free detection of total protein (C). Antibodies: rabbit anti-p53 [p Ser392] (1:1,000, SI-17, NovusBio, U.S.A.) and mouse anti-rabbit HRP-labelled IgG (1: 4,000 HAF0007, R&D Systems, U.S.A.); normalization to the total protein volume (Bio-Rad, U.S.A.)

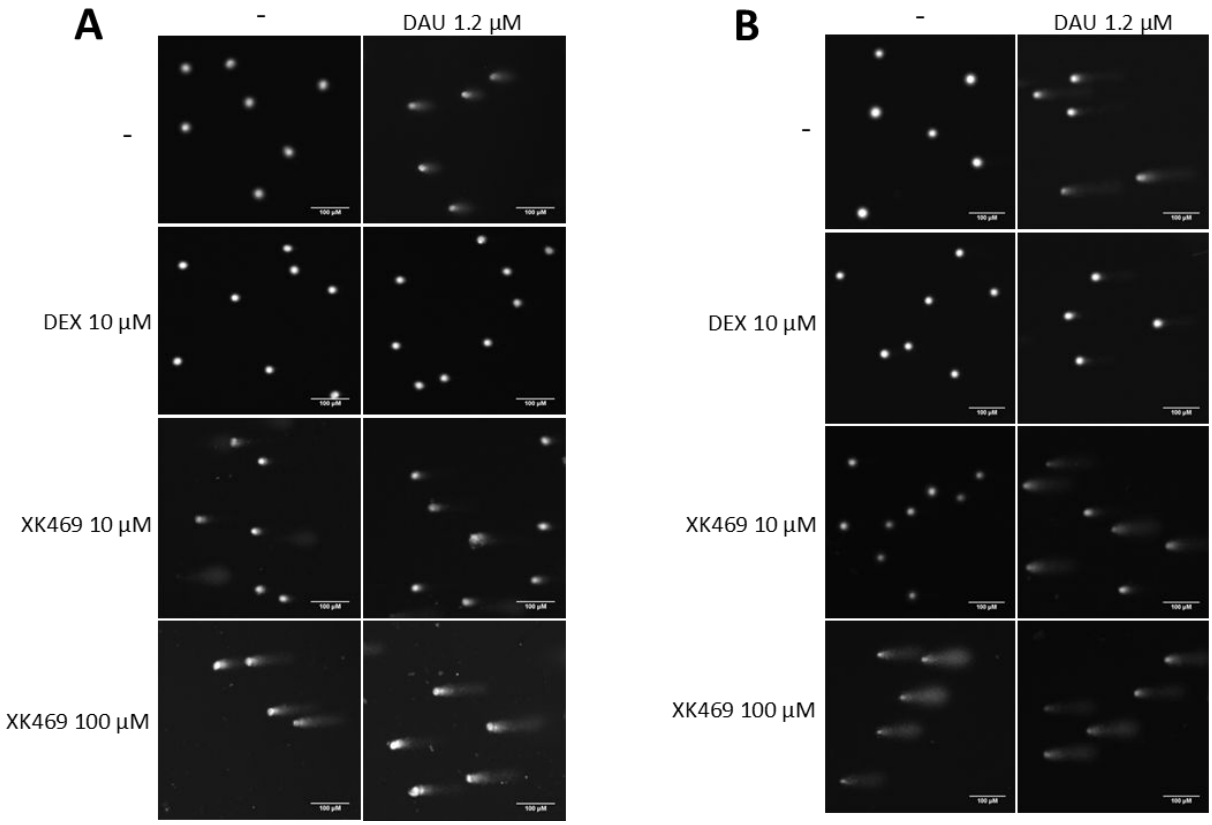

Fig. S7 *DNA damage analysis.* Representative images of Comet Assay performed in primary rat cardiomyocytes (**A**) and HL-60 (**B**). Images were further evaluated using TriTek CometScore Freeware v1.5 for Windows.

A. immunodetection of γH2AX in NVCM

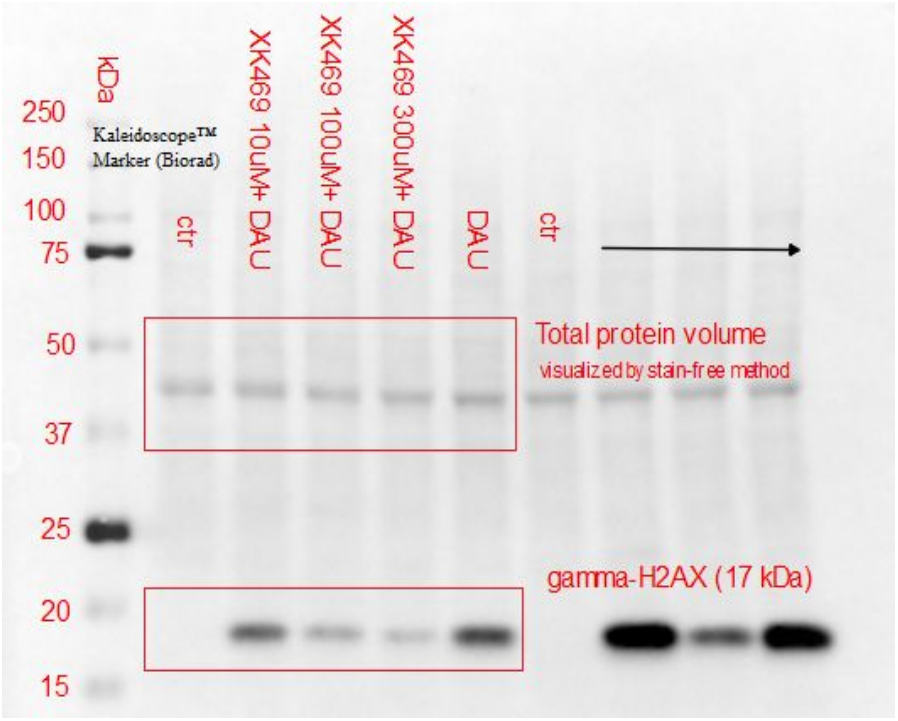

B. chemiluminiscent detection of γH2AX

C. stain-free detection of total protein

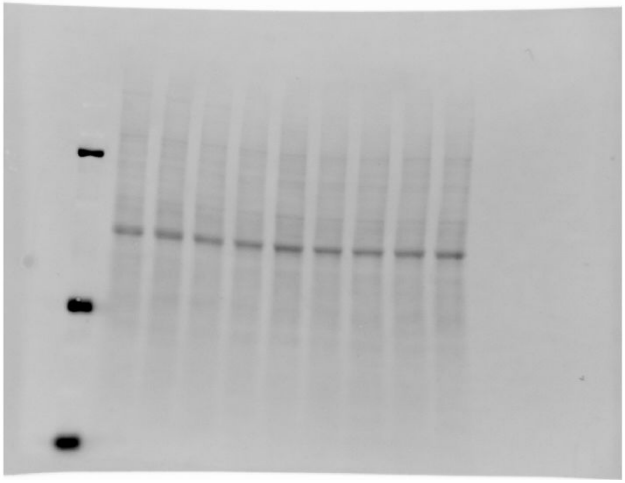

Fig. S8 *Representative membrane of the γH2AX immunodetection in vitro.* Merged signal of chemiluminescence, fluorescent and colorimetric detection (A), chemiluminescent detection of γH2AX (B), stain-free detection of total protein (C). Antibodies: mouse anti-γH2AX (1:5,000; ab11174, Abcam, U.K.) and HRP-labelled anti-mouse IgG (1:40,000; A9044 Merck, Germany); normalization to the total protein volume (Bio-Rad, U.S.A.)

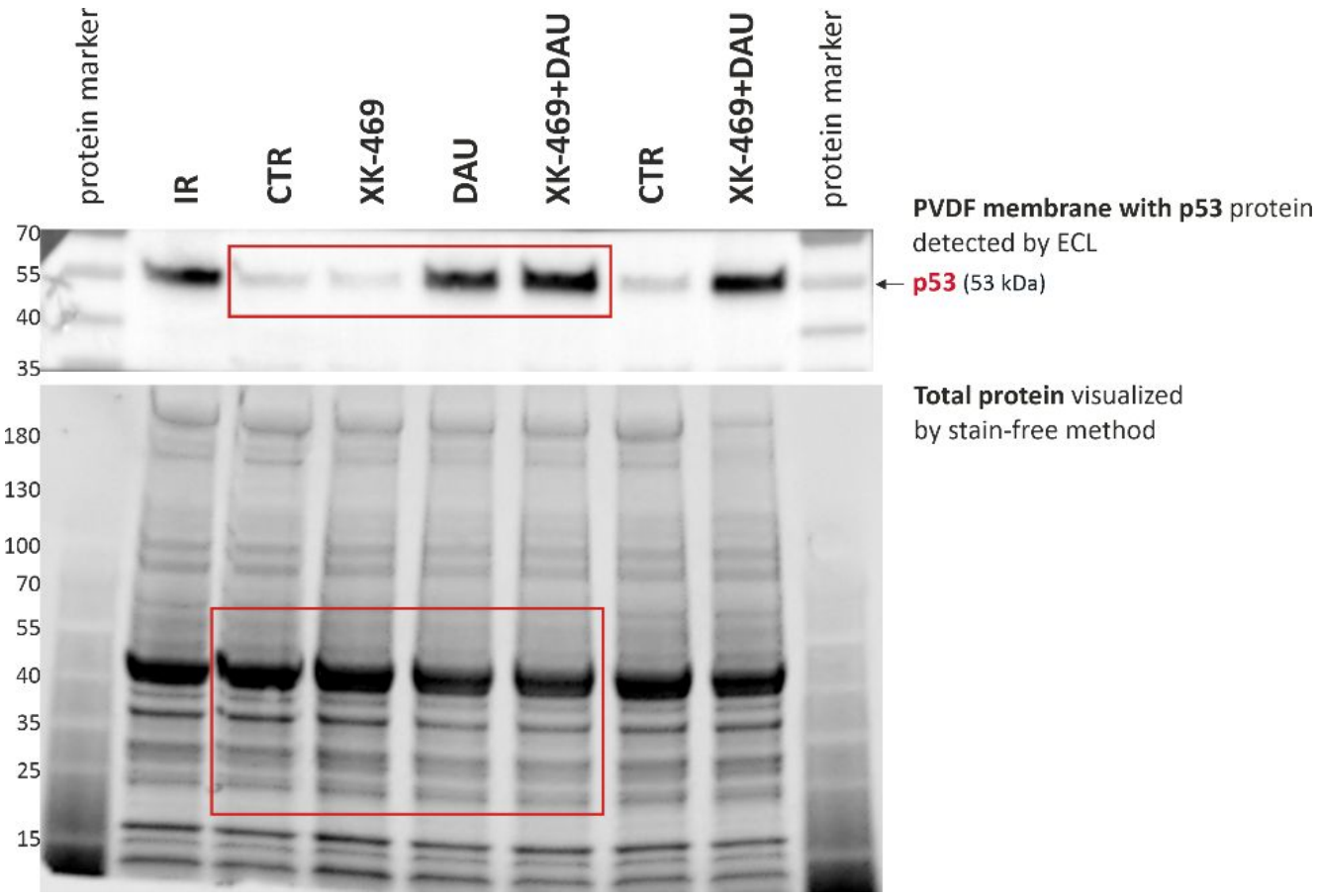

Fig. S9 *Representative gel and membrane of the p53 immunodetection in vivo.* Antibodies: mouse anti-p53 purified primary antibody (1:1,000, BP53-12; Exbio Praha, Czech Republic) and anti-mouse secondary antibody (1:1,000, P0447, Polyclonal Goat Anti-Mouse Immunoglobulin/HRP; DAKO Denmark A/S, Denmark); normalization to the total protein volume (Bio-Rad, U.S.A.)

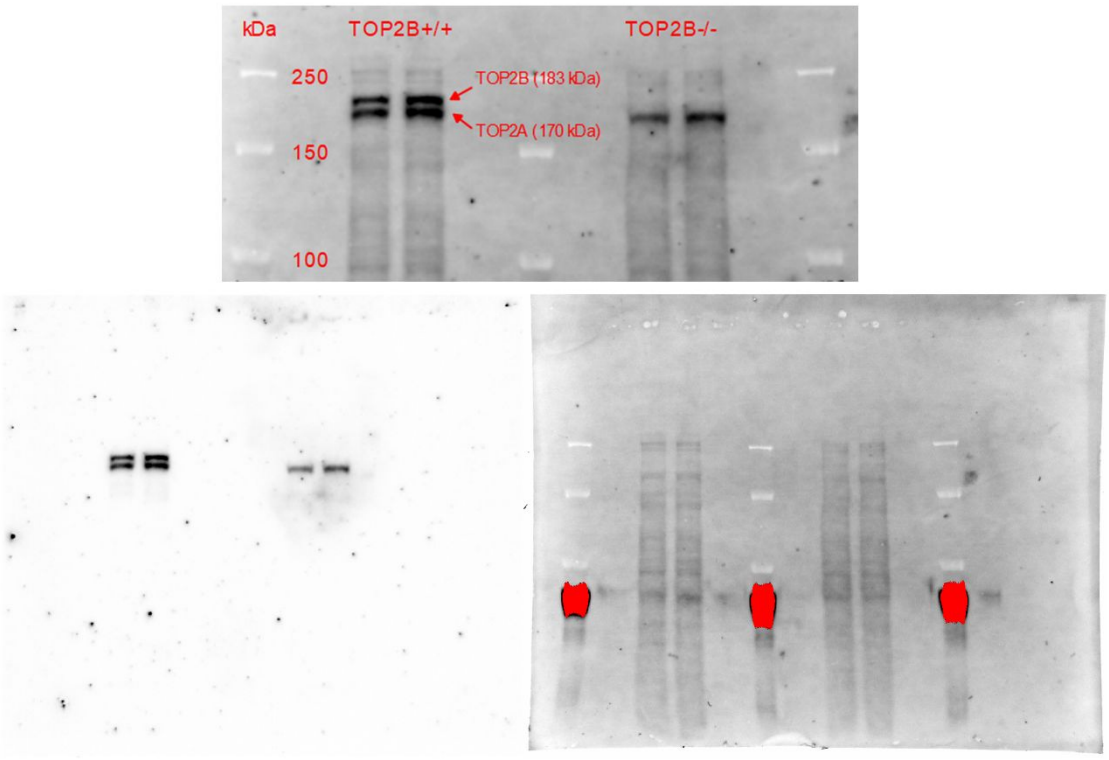

Fig. S10 *Representative membrane of the TOP2 immunodetection in HL-60 cells with TOP2B knocked out by CRISPR-Cas9.* Cell lysis, electrophoresis and immunodetection was performed as for the NVCMs. Merged chemiluminescence and fluorescent image, cropped and annotated (upper panel); chemiluminescent image of TOP2 and stain-free fluorescent image of total protein, both uncropped whole membrane images (lower panels). Antibodies: rabbit anti-TOP2A/B (1: 2,000, ab109524, Abcam, U.K.) and HRP-labelled F(ab')2 goat anti-rabbit IgG (1:10,000, ab6112, Abcam, U.K.).

REFERENCES

Deng J, Feng EG, Ma S, Zhang Y, Liu XF, Li HL, Huang H, Zhu J, Zhu WL, Shen X et al. 2011. Design and synthesis of small molecule rhoa inhibitors: A new promising therapy for cardiovascular diseases? Journal of medicinal chemistry. 54(13):4508-4522.

Hasinoff BB. 2002. Dexrazoxane (icrf-187) protects cardiac myocytes against hypoxia-reoxygenation damage. Cardiovascular toxicology. 2(2):111-118.

Hazeldine ST, Polin L, Kushner J, Paluch J, White K, Edelstein M, Palomino E, Corbett TH, Horwitz JP. 2001. Design, synthesis, and biological evaluation of analogues of the antitumor agent, 2-{4-[(7-chloro-2-quinoxalinyl)oxy]phenoxy}propionic acid (xk469). Journal of medicinal chemistry. 44(11):1758-1776.

Khazeem MM, Casement JW, Schlossmacher G, Kenneth NS, Sumbung NK, Chan JYT, McGow JF, Cowell IG, Austin CA. 2022. Top2b is required to maintain the adrenergic neural phenotype and for atra-induced differentiation of sh-sy5y neuroblastoma cells. Mol Neurobiol. 59(10):5987-6008.

Khazeem MM, Cowell IG, Harkin LF, Casement JW, Austin CA. 2020. Transcription of carbonyl reductase 1 is regulated by DNA topoisomerase ii beta. FEBS letters. 594(20):3395-3405.

Lassagne F, Dugueperoux C, Roca C, Perez C, Martinez A, Baratte B, Robert T, Ruchaud S, Bach S, Erb W et al. 2020. From simple quinoxalines to potent oxazolo[5,4-f]quinoxaline inhibitors of glycogen-synthase kinase 3 (gsk3). Organic & Biomolecular Chemistry. 18(1):154-162.